Nonlinear effects in metals under anomalous-skin conditions

V. T. Dolgopolov

Institute of Solid State Physics, Academy of Sciences of the USSR, Chernogolovka (Moscow Oblast')
Usp. Fiz. Nauk **130**, 241–278 (February 1980)

PACS numbers: 73.25. + i

CONTENTS

1. INTRODUCTION

The appearance of any marked nonlinearity in the electrical properties of normal metals was until recently considered impossible. The only exception was the trivial nonlinearity due to overheating of the metal as a whole. The basis for this view was that the electron system in metals acquires considerable energy even at low electric field strengths because of the high carrier concentrations and the resulting high conductivity. The electron system is not even overheated with respect to the lattice in pure metals under static conditions, since the electrons exchange energy with phonons much more often than with one another. The only consequence of an increase in the field strength would be overheating of the entire metal. Precisely this interpretation was given, for example, to the experimental results of E. S. Borovik, who detected deviations from Ohm's law in bismuth.[1] The nonlinearity was regarded as a result of very slight overheating of the electron system with respect to the crystal lattice that occurred during the overheating of the metal in its entirety.[2,3]

The situation changed with the appearnace of metals of high purity. The magnetic component of the electromagnetic wave took on special importance in these metals. The magnetic field of the wave, which is much larger than the electric field within the metal, produces nonlinearity because the conductivity of pure metals depends on magnetic-field intensity. The first reported observations of this kind of nonlinearity appeared in Refs. 4–6, in which the surface impedance of metals was found to depend on the amplitude of an alternating field. Later discoveries were the generation of the second harmonic and detection of radio-frequency electromagnetic waves by metals,[7-9] both also associated with the magnetic field of the wave.

It is known[10] that weakly damped electromagnetic waves can propagate in pure metals placed in constant magnetic fields. An electromagnetic wave injected into a metal cannot strongly distort the distribution function of all conduction electrons. However, the motion of a small group of electrons responsible for absorption of the wave may be modified noticeably. The result is that at sufficiently high amplitudes, both the Landau damping and the cyclotron damping become functions of wave amplitude.[11-12] The helicon damping function, for example, may be reduced to a small fraction of its normal value as the amplitude rises.

In pure semimetals, where the number of conduction electrons is not as large as it is in a typical metal, it became possible to create high carrier drift velocities in comparatively weak fields. This led to the discovery of a break in the volt-ampere characteristic of bismuth,[13,14] which is due to Cerenkov emission of phonons

 0038-5670/80/020134-22$01.10

when the electron drift velocity exceeds the speed of sound.

We recall, finally, the nonlinearity of the quantizing magnetic field when the amplitude of a radio wave exceeds the period of the quantum oscillations.[15-17]

It is seen from the above enumeration that the manifestations of nonlinearity in normal metals are varied and nontrivial. As a result, the number of papers devoted to their study is increasing steadily. Still, the number of questions that have been posed in the study of nonlinear properties of metals may perhaps exceed the number of answers given. There have been experiments[18-21] for which several equally possible theoretical explanations have been offered.[22-24] There are also experiments[25,26] that have not been interpreted and a number of theoretical predictions[27-28] that have not been verified in experiment.

In this review we examine the causes of a metal's nonlinear response to an external electromagnetic input and the possible manifestations of nonlinearity under conditions for which sufficient clarity has been attained. These conditions include smallness of the frequency ω of the radio wave, $\omega\tau \ll 1$ (τ is the momentum relaxation time of the electron) and the condition $\delta/l \ll 1$, where δ is the depth of the skin layer and l is the carrier free path. This last condition imposes a lower limit on the frequency ω. It is simultaneously a condition for the anomalous skin effect. The anomalous-skin case is of special interest because the radio wave does not interact with all conduction electrons, but only with a small group of them whose motion can be strongly modified by the wave's field. Because of the small number of electrons interacting with the wave, marked nonlinearity appears at a comparatively low radio-wave amplitude, and the manifestations of nonlinearity are numerous and unusual.

Experimental measurements have been made for the most part on bismuth, which is a highly convenient model object. The small cyclotron masses of this metal's electrons enable us to observe nonlinear effects at minimal alternating-field amplitudes. It is further convenient for the comparative simplicity of its Fermi surface and because the linear properties of bismuth have been investigated in exceptional detail. Occasional measurements have been made on typical metals—tin and gallium. In principle, there are no limits on the observability of the effects to be discussed below in metals with high carrier concentrations. It is only necessary to have a large ($l \gg \delta$) electron free path—a property inherent to any pure and perfect metallic crystal at low temperatures.

2. SOURCES OF NONLINEARITY AND OPTIMUM OBSERVING CONDITIONS

a) The equation system

The system of equations that describes the behavior of a metal in an electromagnetic field consists of the Maxwell equations and the material equation that characterizes the properties of the medium. The latter states the relation between the magnitude of the applied field and the current that flows in the metal. It must itself be derived from a microscopic analysis, for example, by solution of the Boltzmann equation:

$$\mathbf{v}\frac{\partial f}{\partial \mathbf{r}} + e\left(\mathbf{E} + \frac{1}{c}[\mathbf{vH}]\right)\frac{\partial f}{\partial \mathbf{p}} = -J(f); \qquad (1)$$

here f is the electron distribution function, E and H are the electric and magnetic field strengths, $J(f)$ is the collision integral [$J(f_0) = 0$, where $f_0 = (\exp[(\varepsilon - \varepsilon_\Phi)/k_B T] + 1)^{-1}$ is the Fermi function corresponding to the lattice temperature]. The field H includes both the constant field and the field of the electromagnetic wave.

The Boltzmann equation is a nonlinear integrodifferential equation. Nonlinear effects are usually (see, for example, Ref. 29) assumed to be weak and this equation is linearized. It is assumed that the distribution function changes little from its equilibrium value $f = f_0 + g$ ($g \ll 1$) and by representing Eq. (1) in the form

$$e\mathbf{E}\frac{\partial f_0}{\partial \mathbf{p}} + \mathbf{v}\frac{\partial g}{\partial \mathbf{r}} + e\left\{\mathbf{E} + \frac{1}{c}[\mathbf{v}(\mathbf{H}_\sim + \mathbf{H})]\right\}\frac{\partial g}{\partial \mathbf{p}} = -J(f), \qquad (2)$$

the terms $e\mathbf{E}\partial g/\partial \mathbf{p}$ and $(e/c)[\mathbf{vH}]$ responsible for the nonlinearity are omitted and the exact notation for the collision integral, also a source of nonlinearity, is replaced by the model notation $J(f) = g/\tau$. Then the electric current density $\mathbf{j} \sim \int e\mathbf{v}\, g\, d^3p$ is proportional to the magnitude of the electric field E.

The standard procedure for solution of Eq. (2) with nonlinear terms consists of expanding the electromagnetic fields and the increments to the distribution function in series in harmonics of the fundamental frequency:

$$E = E_1(\omega) + E_2(2\omega) + \ldots,$$
$$H_\sim = H_1(\omega) + H_2(2\omega) + \ldots,$$
$$g = g_1(\omega) + g_2(2\omega) + \ldots,$$
$$E_1(\omega) \sim \cos\omega t \sim (e^{i\omega t} + e^{-i\omega t}).$$

Then $g_n \sim E_n \sim H_n \sim E_1^n$, so that successive approximations can be used for solution, isolating the terms of the equation that correspond to higher harmonics of the frequency ω. We note that g_2 also contains the increment for the rectified current, since it has a term g_0 that does depend on ω and is proportional to the product $e^{i\omega t}e^{-i\omega t}$. This term will be of special interest to us later on, since most of the effects to be examined below are involved with the detection of alternating currents in metals.

Instead of all the terms responsible for nonlinearity in the equation for an n-th harmonic, it is convenient to retain only those that are the main sources of nonlinearity. Their relative magnitudes can be estimated with this in mind, and the largest ones selected. (Below we shall be interested only in the equation for the second harmonic of the frequency ω; we shall therefore make all estimates for this equation). The relative magnitudes of the various terms must be compared quite painstakingly, since it may be that a given term predominates for a small electron group but this group itself makes no appreciable contribution to the current of the corresponding harmonic. Moreover, a term associated with the magnetic field has no effect at all on the isotropic part $g = g(\varepsilon)$ of the increment to the distribution function, i.e., the part that depends only on energy. Below we shall discuss whether it is possi-

ble to create a large isotropic distribution-function increment (to "overheat" the electron system) in metals, but we now assume for the time being that the distribution-function increment is basically anisotropic.

b) Case of an anisotropic increment to the distribution function

Let us estimate the magnitudes of the three Boltzmann-equation terms that are responsible for nonlinearity. We first compare $a_1 = eE_1 \partial g_1/\partial p$ and $a_2 = (e/c)[\mathbf{v}\mathbf{H}_1]\partial g_1/\partial p$. In the case of the normal skin effect, the electron distribution shifts periodically as indicated in Fig. 1. The increment to the distribution function for the fundamental is of the order of $g_1 \sim (\partial f_0/\partial\varepsilon)\Delta\varepsilon \sim eE_1 l_{tr}/k_B T$ ($l_{tr} = v\tau_{tr}$ is the transport electron free path). In momentum space, g_1 decreases to zero over a distance (see Fig. 1) of the order of $\Delta p \sim k_B T/(\partial\varepsilon/\partial p) \sim k_B T/v$ (v is the Fermi velocity). Therefore $a_1 \sim (eE_1 l_{tr}/k_B T)^2 \tau_{tr}^{-1}$. The component $\partial g_1/\partial p$ perpendicular to the electron velocity is included in a_2 and is of the order of g_1/mv, where m is the electronic mass. The ratio a_1/a_2 therefore equals $a_1/a_2 \sim (c/v)(E_1/H_1)\varepsilon_F/k_B T \sim (\omega\delta/v)\varepsilon_F/k_B T$, where we have recognized that $E_1(\omega) \sim (\omega/c)\delta H_1$.

In a typical metal at $\varepsilon_F \sim 10$ eV, according to this estimate, the contributions to nonlinearity from the electric and magnetic fields of the wave become equal (at temperatures of the order of 1 K) at frequencies $\omega \sim 10^9$. The contribution from the magnetic field of the wave prevails at lower frequencies.

Under anomalous-skin-effect conditions, the distribution function changes appreciably only in a narrow range of angles α near the points of the Fermi surface at which the electron velocity is parallel to the surface of the specimen (Fig. 2). These "effective" electrons make the basic contribution to the conductivity. In the absence of a constant magnetic field, the angle range α is of the order of δ/l. (Here $l = v\tau$ is the path length for small-angle scattering. If the electrons are scattered for the most part by impurities or vacancies, l and l_{tr} are the same. If, on the hand, scattering by phonons prevails, we have $l < l_{tr}$ at low temperatures). In a magnetic field, $\alpha \sim \sqrt{\Delta/r}$, where $r = vmc/eH$ is the radius of the Larmor orbit of the electron ($\delta \ll r \ll l$).

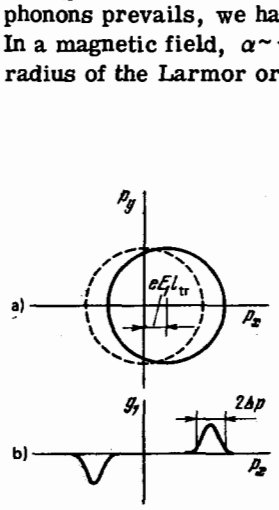

FIG. 1. Change of skin-layer electron distribution in the case of the normal skin effect. a) Plot for $f(\varepsilon) = \text{const} < 1$; b) increment to equilibrium distribution function $g_1(p_x)$ at $p_y = 0$.

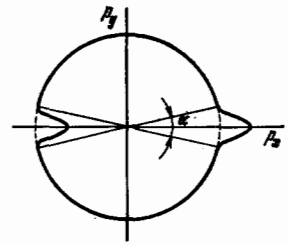

FIG. 2. Skin-layer electron distribution function for a case of the anomalous skin effect. Plot for $f(\varepsilon) = \text{const} < 1$.

Because α is small, a_2 increases further in the anomalous skin effect. In this case the ratio a_1/a_2 will decrease still further: $a_1/a_2 \sim \alpha\varepsilon_F\omega\delta/vk_B T$. At $\omega\tau \ll 1$, the ratio $a_1/a_2 \ll 1$ down to temperatures of the order of 0.1 K. In general, the temperature dependence is of a random nature in this estimate and results from the fact that we are estimating the ratio of single terms in the kinetic equation and not the ratio of the corresponding currents.

It is somewhat more difficult to estimate the contribution of the collision integral to the nonlinear effects. This contribution appears as a consequence of the Pauli principle. The collision integral has the form

$$J = \frac{2}{(2\pi\hbar)^3}\int [(1-f_{p'})f_p w_{pp'} - f_{p'}(1-f_p)w_{p'p}]\,d^3p'. \qquad (3)$$

If $w_{pp'} = w_{p'p}$, as in the case of scattering by impurities and defects, the products $f_{p'}f_p$ drop out of the collision integral. Therefore scattering on these centers does not result in nonlinear dependence of the collision integral on the applied fields. It is a different matter when we come to electron scattering by phonons. Since the probability of absorption of a phonon with wave vector $\mathbf{q}$ is proportional to the number of phonons $N(q)$ and the probability of emission of such a photon is proportional to $N(q)+1$, $\omega_{pp'} \neq \omega_{p'p}$, and the integral for collisions on phonons contains a term that depends on the product $g(\mathrm{p})g(\mathrm{p}')$:

$$a_3 \sim \frac{\Delta^2 g(p)}{8\pi^3 N_a M_a s^2}\int qg(\mathbf{k}')\,\delta(\varepsilon_{\mathbf{k}'} - \varepsilon_{\mathbf{k}'+\mathbf{q}} + \hbar qs)\,d^3k' \sim \frac{g_1^2}{\tau_{eph}}\alpha, \qquad (4)$$

where N_a is the number of atoms per unit volume, M_a is the mass of the atoms, s is the speed of sound, α is the angle interval in p-space, in which $g_1(p)$ is nonzero, and Δ is the deformation potential.

The time τ_{eph} is the total time of electron-phonon scatscattering and is related to the transport relaxation time by $\tau_{eph} = \tau_{eph}^{tr}(T/\theta)^2$, where θ is the Debye temperature. The time τ_{eph} can be measured experimentally by studying the temperature dependence of such effects as cyclotron resonance or the radio-frequency size effect, in which small-angle scattering of electrons is significant.

In real metals at temperatures around 4K, τ_{eph} is of the order of τ.[30] This implies that $a_3 \sim a_1$ in the normal skin effect, while $a_3 \ll a_1$ under anomalous-skin conditions. We shall not consider the case of electron-electron scattering, since $\tau_{ee} \gg t_{eph}$ in all metals, except perhaps for the transition metals.

c) The possibility of overheating of the electron system in metals

To obtain a "warm" electron system in a metal, i.e., a perturbed electron system whose distribution function $g(\varepsilon)$ has an isotropic part, it is necessary that momentum relaxation of the electrons occur much more rapidly than their energy relaxation. The electron system loses energy at low temperatures by emitting acoustic phonons. In each phonon-emitting event in a typical metal, the electron loses the entire energy excess that rendered it nonthermal. Therefore the largest momentum that an emitted phonon can have is the Fermi momentum, and the energy of this phonon is of the order of $k\theta$, so that the electron can lose smaller energies in a single phonon-emission event. As a result, the energy relaxation time τ_e is of the same order as the electron-phonon scattering time $\tau_{eph}(\varepsilon)$ and in pure metals is equal to or even smaller than the momentum relaxation time.

Momentum relaxation of the electrons can be accelerated by injecting impurity atoms into the metal. Since scattering on impurities is elastic, there is no change in the energy relaxation of the electron system due to introduction of the impurity, and the condition $\tau_e \sim \tau_{eph} \gg \tau$ will be satisfied. The electron-electron scattering time is quite short in transition metals (see, for example, Ref. 31), $\tau_{ee} \ll \tau_e$. In this case, intensive energy exchange between electrons will result in establishment of thermal equilibrium in the electron system. The time ratio is inverted for other metals, $\tau_e \sim \tau_{eph} \ll \tau_{ee}$; therefore thermal equilibrium is not established in the electron system. Nevertheless, we shall use the electron temperature T_e below for order-of-magnitude estimates, remembering that the electron system is markedly perturbed in low-frequency fields only near the Fermi level and that the isotropic part of the distribution function can be represented approximately in the form $f_0 + (\pi^2/6)(k_B T_e)^2 \partial^2 f_0/\partial\varepsilon^2$.

In semimetals, where the dimensions of the Fermi surface are small, energy relaxation can take place much more slowly than momentum relaxation even in the absence of an impurity. If the characteristic dimension of the Fermi surface is p_F, cooling of the electron system at $k_B T_e \gtrsim k_B T > p_F s$ will take place by emission of phonons with energy of the order of $p_F s$. At temperatures $k_B T \gg p_F s$, it becomes difficult for the electrons to lose energy because the probabilities of phonon absorption and emission become equal.[32]

In fact, the number of phonons with energy of the order of $p_F s$ is proportional to the Bose-Einstein distribution function:

$$N \sim (e^{-\mu_{ph}/k_B T} - 1)^{-1} \sim \frac{k_B T}{\mu_{ph}} \gg 1. \qquad (5)$$

Therefore the probability of emission of a phonon with energy $p_F s$, which is proportional to $N+1$, is almost equal to the probability of absorption of the same phonon, which is proportional to N. In other words, one electron-system energy-loss event occurs, on the average, every $(2N+1)$ events in which electrons are scattered by phonons with loss of momentum. The energy lost by the electron system in a unit volume per unit time has the form $p_F s(p_F s/k_B T \times k_B[(T_e - T)]\tau_{eF}^{-1}]n/\varepsilon_F$, where we have taken into consideration that the fraction of electrons capable of losing energy by phonon emission is of the order of $k_B(T_e - T)/\varepsilon_F$ of the total number n of electrons in the unit volume. The loss of energy by the electron system can be represented in the form $\delta\varepsilon/\tau_e$; here $\delta\varepsilon \sim k_B^2(T_e^2 - T^2)n/\varepsilon_F$. Equating the two expressions for the power lost by the electrons, we find $\tau_e \sim (k_B T/p_F s)^2 \tau_{eF} \gg \tau_{eF}$. This relation was derived more rigorously by Greene.[33]

If the Fermi-surface area under consideration has the form of a long, slender ellipsoid, a similar relation between the momentum and energy relaxation times may be preserved in a quantizing magnetic field down to very low temperatures of the order of Ps/k, where P is the smallest dimension of the ellipsoid. To verify this, let us assume that the electron spectrum of the metal is square-law, $\varepsilon = (p_x^2 + p_y^2)/2m + (p_z^2/2M)$, and that the effective masses m and M differ greatly, $M \gg m$. The Fermi surface then has the form of an ellipsoid of revolution, with the z axis a long one. The magnetic field H is directed along this axis. In the quasiclassical approximation, the allowed states in momentum space are located on cylindrical tubes whose axes are parallel to the magnetic field (Fig. 3).

We shall confine ourselves to examination of the electrons on the tube tangent to the original Fermi surface at $p_z = 0$. States in the range $2\Delta p \sim 2\sqrt{2k_B T_e M}$ are occupied on this tube. Since quantization assumes that $\hbar\Omega = \hbar(eH/mc) \gg k_B T_e$, transitions from one tube to another without a change in p_z are impossible by virtue of the Pauli principle. Electron scattering could take place along the Fermi surface. However, we shall assume that the distance p_1 to the nearest tube, found from the condition $p_1^2/2M = \hbar\Omega(p_1 \gg \Delta p)$, may be considerably larger than the phonon momentum, $p_1 \gg k_B T_e/s$. In other words, we shall assume satisfaction of the following chain of inequalities:

$$\varepsilon_{ph} \gg \hbar\Omega \gg \frac{(k_B T_e)^2}{Ms^2} \gg \frac{m}{M}\varepsilon_{ph} \quad T_e \gtrsim T. \qquad (6)$$

When these inequalities are satisfied, electrons are scattered only within a single cylindrical tube, whose characteristic dimensions are small compared to the

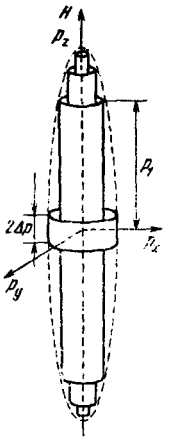

FIG. 3. Electron spectrum in quantizing magnetic field.

thermal-phonon momentum. For the reasons discussed above, we must also expect $\tau_e \sim (k_B T/Ps)^2 \tau_{eph}$ in this case. This problem is discussed in greater detail in Ref. 34.

Real metals have, in addition to areas with small Fermi-surface dimensions, large surface areas on which electron energy relaxation takes place quickly. Therefore mixing of electrons of various groups, i.e., transitions between different areas of the Fermi surface, even if it occurs as a result of impurity scattering and the energy of the scattered electron is conserved, are capable of reducing the energy relaxation time of the electrons of the group considered.

It has been assumed up to this point that the temperature of the phonon system remains unchanged. Let us now establish the conditions under which the phonon system would be able to act as a thermostat. Let us estimate the characteristic relaxation time τ_{ph} of the phonon system. In a typical metal, the energy yielded by an electron in a single phonon-emission event is of the order of $k_B T_e$; therefore a power $k_B T_e n[k_B(T_e - T)/\varepsilon_F \tau_{eF}] = u$ is transferred to the phonon system per unit volume. This power is expended to increase the temperature of the phonon system, $u = k_B n(T/\theta)^3\, dT/dt \sim k_B n(T/\theta)^3 (T_e - T)/\tau_F$. Therefore[3] $\tau_F \sim \tau_{eF}(\varepsilon_F/k_B\theta)(T/\theta)^2$. At frequencies $\tau_3 \ll \omega^{-1} \ll \tau_F$, the phonon system has only a mean heating determined by the thermal balance of the crystal, while the electron-system temperature oscillates at frequencies that are multiples of ω. The temperature of the entire crystal as a whole may oscillate at $\tau_{ph} \ll \omega^{-1}$.

In semimetals, where the number of electrons n is small compared with the number of crystal-lattice atoms N_a per unit volume, $\tau_{ph} \sim (N_a/n)\tau_{eF}(\varepsilon_F/k_B\theta)(T/\theta)^2$. Therefore, $\tau_{ph} \gg \tau_e$ down to temperatures ~1K.

Let us now estimate the possible contribution of electron-system overheating to nonlinear effects. We shall assume that $\tau \ll \tau_3 \ll \omega^{-1} \ll \tau_F$. Since we are interested only in estimating the isotropic part of the distribution-function increment, we shall use the budget of the energy coming in to and going out from the electron system instead of solving system (2) for the isotropic and anisotropic parts of g.[35] A power $\sim \delta\omega H_1^2/4\pi$ crosses a unit area of the surface into the specimen. The average distance in which the electron loses its energy is $l_e \sim l\sqrt{\tau_e/\tau}$ in the absence of constant magnetic field and $l_e \sim (v/\Omega\sqrt{\tau_e/\tau}$ in a strong magnetic field, where $\Omega\tau \gg 1$. In the simplest situation of the normal skin effect, in which the condition $l_e \ll \delta$ is satisfied, the energy acquired by the electron system is transferred to phonons within the skin layer. The energy balance then gives

$$\omega\delta \frac{H_1^2}{4\pi} = \frac{\partial n}{\partial \varepsilon} \frac{k_B^2 (T_e^2 - T^2)}{\tau_e} \delta. \tag{7}$$

Therefore at $T_e - T \ll T$ we have $T_e - T \sim k_B^{-1}(3/8\pi)(H_1^2/n)(\varepsilon_F/k_B T) \times \omega\tau_e$. The term $a_4 = v\partial g_\pi/\partial r \sim v(\partial f_0/\partial T)\nabla T_e \sim (eE_1 l_{tr}/k_B T)^2 \tau_{tr}^{-1}(\tau_e/\tau_{tr}) \times (l_{tr}/\delta)$ will appear in the equation for the anisotropic part of the distribution function. The ratio $a_4/a_2 \sim \omega\tau_e\varepsilon_F/k_B T$ may be large at comparatively low frequencies, so that allowance for overheating is essential in the study of nonlinear properties under conditions of the normal skin effect with $l_e \ll \delta$.

A different relation between l_e and δ is possible in the normal skin effect: $l \ll \delta \ll l_e$. As far as overheating of the electron system is concerned, this case differs in no way from that of the anomalous skin effect. In the right-hand side of (7), δ will now be replaced by l_e, and at a given H_1 the difference between the electron and lattice temperatures will be lowered by a divisor l_e/δ; the temperature gradient will also be lowered by the same divisor. As a result, $a_4/a_2 \sim \omega\tau(\varepsilon_F/k_B T)(\delta/l)\delta/l_e \ll 1$, and the manifestations of electron-system overheat will be weak under these conditions.

d) Conditions of observation

The net result of the above analysis is that the magnetic field of the wave is the principal source of nonlinearity in pure metals at $\omega\tau \ll 1$. Let us now attempt to find the conditions under which nonlinear phenomena can be observed at the lowest radio-wave amplitude. To this end, we shall find the characteristic amplitude h of the radio wave incident on the metal beginning at which the nonlinearity becomes appreciable for various cases. (In the case of weak nonlinearity, the fields and currents can be represented in series form in H_1/h.)

1) *Weak constant magnetic field* $H < H_1$. Under the conditions of the normal skin effect, nonlinearity appears as a result of the influence of the wave's magnetic field on conductivity. The dependence of conductivity on the magnetic field will become strong when $\Omega\tau_{tr} = (eH_1/mc)\tau_{tr} \gg 1$, so that the characteristic amplitude of the alternating field is

$$h_\pi = \frac{mc}{e\tau_{tr}}. \tag{8}$$

In the anomalous skin effect, the influence of the wave's magnetic field comes into play as soon as the path length of the effective electron within the skin layer becomes smaller than the free path and effective electrons can escape the skin layer in the interval between two scattering events. The electron path length in the skin layer is $2\sqrt{2\delta v/\omega}$. Equating this to the free path l, we obtain

$$h_a = 8\frac{mc}{e\tau}\frac{\delta}{l}. \tag{9}$$

2) *Quantizing magnetic field*: Because of the Shubnikov-de Haas effect, the conductivity of a metal oscillates on variation of the magnetic field. We may expect the appearance of noticeable nonlinearity when the wave amplitude is comparable to the period of the oscillations. We find the shortest period from the quantum level resolvability condition $\hbar\Omega \sim 2\pi^2 k_B T$. Therefore

$$h_\pi \sim \frac{mc}{e\hbar}\frac{(\hbar\Omega)^2}{\varepsilon_{ph}} \sim \frac{mc}{e\hbar}\frac{(\pi^2 k_B T)^2}{\varepsilon_{ph}}. \tag{10}$$

Numerical estimation of these characteristic values of h from formulas (8)–(10) indicates that the weakest requirements on the amplitude of the alternating field at $T \sim 1$ K apply in a small constant magnetic field in the anomalous skin effect. The entire exposition that follows is devoted to this case.

The value of h_a is not large. By way of example, we

cite figures for bismuth. The lightest carrier mass $m \sim 10^{-29} g$, the carrier free path at helium temperatures $l \sim 10^{-1}$ cm, $v \sim 10^{8}$ cm/sec, and the depth of the skin layer at 1 MHz is of the order of 10^{-3}cm, so that $h_a \sim 10^{-2}$ Oe. Other conditions the same, the effective electron masses in a typical metal are a hundred times larger, but then the depth of the skin layer is an order of magnitude smaller, owing to the increased number of carriers; therefore $h_a \sim 10^{-1}$ Oe.

3. NONLINEAR SIZE EFFECT

a) Qualitative discussion

Let us begin by considering the simplest case of nonlinearity under the conditions of the anomalous skin effect, namely the case in which the alternating-field amplitude at the surface of the metal is small compared to the external constant magnetic field H_0. Then the electron paths are shaped by the constant magnetic field, and the wave magnetic field merely distorts them weakly inside the skin layer. We shall assume satisfaction of the inequalities $\omega\tau \ll 1 < \Omega\tau$, $\delta \ll r = v/\Omega$. It can be assumed under these conditions that the electrons move in a quasistatic but spatially strongly nonuniform electromagnetic field. Since the phase shift between the alternating electric $E_1(\omega)$ and magnetic $H_1(\omega)$ fields differs from $\pi/2$, the intrinsic magnetic field of the wave, which is superimposed on the constant magnetic field H_0, results in nonequivalence of the two half-periods of the alternating current. The half-period nonequivalence is due to the change in the effective-electron path in the skin layer. As a result, an electric current that is proportional to the product $M_1 E_1$ and has a constant component appears at the surface of the specimen. The rectified current is spatially inhomogeneous; it is damped out at a distance of the order of δ from the surface. It is easy to obtain an estimate for the direct-current density j_2 if the field H_0 is parallel to the surface of the metal. The high-frequency current $j(\omega)$ is proportional to $\sigma_0 E_1 \delta r^{-1}$, where σ_0 is the static conductivity. We take the wave magnetic field into account as follows: $j_2 \sim H_1 dj_1/dH_0$. Using the estimate $H_1 \sim cE_1/\omega\delta$, we obtain $j_2 \sim \sigma_0 E_1 (\omega\tau)^{-1} eE_1 l \varepsilon_F^{-1}$.

It is known[36] that spikes of high-frequency current may appear in the interior of the metal under the conditions of the anomalous skin effect in the presence of a constant magnetic field; they are due to the ballistic motions of electron of the extremal sections of the Fermi surface. We may expect the presence of a direct current concentrated at the specimen's surface to result similarly in the appearance of direct-current spikes inside the specimen. In general, any nonuniform field distribution may be transported by electrons. For example, the transport of inhomogeneous deformations in metals along a chain of paths has recently been observed.[37-39] However, the transport of an inhomogeneous direct current has certain specific properties. This is because the appearance of a direct-current spike is not generally associated with the appearance of a constant electric field. To verify this it suffices to imagine a metallic specimen occupying the half-space $z > 0$ and apply one of the Maxwell equations in integral form:

$$\oint \mathbf{E}\, d\mathbf{r} = -c^{-1} \frac{\partial}{\partial t} \int H_n \, df. \tag{11}$$

The contour of integration is indicated in Fig. 4. Since $E = 0$ in the interior of the metal and the average value of the time derivative of the magnetic flux, taken over times that are larger than ω^{-1}, also vanishes, we find at once that the inhomogeneous direct current is not coupled to the appearance of a constant electric field under these conditions. Because of the absence of electric field in the spike, the spike may be transported only to the distance reached directly by the electrons present in it. In other words, chains of direct-current spikes cannot arise as a result of the transport of direct current along a chain of orbits. Nevertheless, chains of direct-current spikes do exist. These results from transport of the fundamental current and nonlinear effects in deep spikes of that current along a chain of orbits.

This occurs as follows. In a magnetic field parallel to the surface of the metal, electrons of an extremal Fermi-surface cross section, while in the skin layer, are refocused at depth $2r$ in their path motion and reproduce the direct-current spike at this depth. At the same distance from the surface there is a spike of the fields H_1 and E_1, which results in the appearance of direct current at depths $2r$ and $4r$, and so forth. It is clear from these arguments that a similar system of spikes will also appear for the current $\tilde{j}_2$ at frequency 2ω.

In a specimen of limited size, the presence of a system of direct-current spikes, the distance between which is determined by the external magnetic field H_0, should result in the appearance of a nonlinear size effect similar to the radio-frequency size effect.[36] The nonlinear size effect appears as a singularity in the magnetic moment of a plate when the external magnetic field reaches values $H_N = N 2vmc/ed$, where d is the thickness of the plate and N is an integer. The magnetic moment itself arises as a result of detection of the alternating field in the skin layer and deep spikes in the interior of the specimen.

Penetration of a direct-current spike into the opposite skin layer is not the only cause of the nonlinear size effect. In the magnetic field in which the diameter of the electron orbits is equal to the thickness of the specimen, the contribution to the size effect at a current j_2 proportional to $E_1(0)E_1(1)$ [where $E_1(N)$ is the amplitude of the high-frequency field in the N-th spike] changes the number of returns of electrons into the skin layer

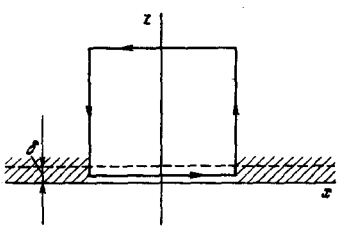

FIG. 4. Contour of integration in (11).

as a result of scattering of electrons by the opposite side of the plate. The size of this contribution is determined by the degree of specularity of electron scattering on the specimen surface. However, the cutoff of electron orbits cannot contribute to the nonlinear size effect in fields corresponding to agreement of specimen thickness with several electron-orbit diameters.

An incremental direct current proportional to $E_1(0)E_1(N)$ also appears in the skin layer when the next spike of the high-frequency field emerges at the surface. The contributions to the nonlinear size effect from surface crossings of high-frequency and direct-current spikes are identical in order of magnitude and cannot be distinguished experimentally. In any event, the linewidth of the nonlinear size effect will be determined by the depth of the skin layer at frequency ω, so that an increase in the frequency of the alternating field should result in narrowing of the lines.

b) Structure of direct-current spikes

The distribution of the direct current in the spikes is calculated by successive approximations as set forth in paragraph a) of Sec. 2. The corresponding equations for the distribution-function increments responsible for the fundamental and direct currents have the form

$$v_z \frac{\partial f_1}{\partial z} + \Omega \frac{\partial f_1}{\partial \varphi} + \tau^{-1} f_1 = eE_1 v, \tag{12}$$

$$v_z \frac{\partial f_2}{\partial z} + \Omega \frac{\partial f_2}{\partial \varphi} + \tau^{-1} f_2 = -\frac{e}{2mc} \operatorname{Re}\left(H_1 \frac{\partial f_1^*}{\partial \varphi}\right), \tag{13}$$

where the asterisk identifies the complex conjugate and $g_1(\omega) = f_1 \partial f_0 / \partial \varepsilon$, $\varphi = \Omega t$ is the dimensionless time of electron motion on the orbit. It is assumed that the metal occupies the half-space $z > 0$ and that the electric field E_1 is oriented along the x axis and the constant magnetic field H_0 along the y axis. The solution of Eq. (12) is well known (see, for example, Refs. 40, 36). The electric field $E_1(z)$ penetrates into the specimen, forming spikes at values of z that are multiples of $2r = D$.

Equation (13) has been solved[9] for the case of a cylindrical Fermi surface with a cylinder axis parallel to the external magnetic field. Rather unwieldy calculations yield the following expression for the current density:

$$j_2(z) = \frac{\sigma_0 \delta}{2\pi \omega p} \operatorname{Im}\{2E_1(z)\,\widetilde{E}_1^*(z) + E_1(z)\{E_1(z-2r) - E_1^*(z+2r)\}\}, \tag{14}$$

$$\widetilde{E}_1(z) = \pi^{-1} \int_0^\infty \sin(qz)\, E_1(q)\, dq, \quad r = \frac{v}{\Omega},$$

where $E_1(q)$ is the Fourier component of the field of the fundamental. The value of the current j_2 agrees with the estimate obtained earlier by a qualitative procedure. The distribution of the direct current over the thickness of the specimen can be found at an arbitrary z by using the $E_1(z)$ relation given in Ref. 40. This distribution is shown schematically in Fig. 5.

Antisymmetric direct-current spikes appear at values of z that are multiples of $D = 2r$. At large numbers N, the amplitude of the spikes decreases as $N^{-2/3}$, and the signs of the spikes alternate. No constant electric field appears, but the current j_2 gives rise to a constant magnetic field $\mathcal{H}$ whose magnitude, accurate to a numerical multiplier of the order of unity, is $H_1^2(0)/(2\pi)^3 H_0$, while its direction is the opposite of that of the external magnetic field H_0.

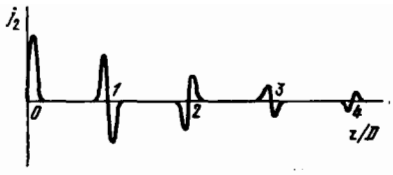

FIG. 5. Direct-current density j_2 vs. distance to surface of metal.

It is seen from the structure of relation (14) that the magnitude of the rectified current in the N-th spike is sensitive only to the magnitude of the electric field in its nearest neighbors. This corresponds at once to the absence of direct-current-spike transport along a chain of electron paths.

c) Experimental observation of nonlinear size effect

The semimetal bismuth is thus far the only object in which the nonlinear size effect has been observed, although there is no reason to assume that it would be any more difficult to observe it in metals with high carrier concentrations. This is because the power released in the specimen is proportional to $H_1^2\delta \sim H_1^2 n^{-1/3}$, so that the field H_1 can be increased by a factor $n^{1/6}$ at a given specimen overheat with respect to the helium bath. Since the magnetic moment of the specimen is of the order of H_1^2/H_0, and the field H_0 in which size-effect lines are observed is proportional to $n^{1/3}$, a magnetic moment of the same magnitude as in bismuth can be obtained in this field without increasing the overheat of the specimen.

The most direct method of observing the nonlinear size effect would be direct measurement of the magnetic field in the interior of the specimen as a function of the magnitude of the external magnetic field. However, actual measurements have been made differently.[9] A modulation technique has been used that makes it possible to raise the sensitivity of the instruments significantly.

A specimen in the form of a plane-parallel plate was placed within a system of three induction coils as indicated in Fig. 6. The induction-coil system was placed directly in the helium bath together with the specimen. One of the coils (coil 3 in Fig. 6) was used to create an alternating electromagnetic field in the frequency range 0.5–2.5 MHz with amplitudes $H_1(0)$ up to 5 Oe. The overheat of the specimen relative to the helium bath did not exceed 0.2 K at these magnetic-field amplitudes. The other two coils formed a bridge circuit operating at frequencies from 100 to 1000 Hz. At frequencies below 1000 Hz, the alternating magnetic field was practically uniform through the thickness of the specimen. The amplitude $H_{\sim}$ of the low-frequency alternating field was 0.1 Oe.

The signal from the receiving coil went to a filter that suppressed the high frequency, and then, after

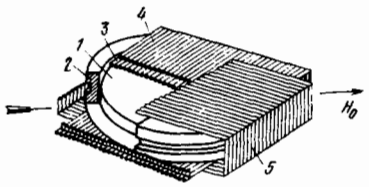

FIG. 6. Diagram showing measuring-coil arrangement. 1) Specimen; 2) rotating base; 3) high-frequency induction coil; 4 and 5) low-frequency coils.

narrow-band amplification and synchronous detection, to the y-coordinate of an automatic-recording potentiometer. A voltage proportional to the constant magnetic field H_0 was applied to the potentiometer's x-coordinate. The magnetic field H_0 was parallel to the plane of the specimen.

The electronic radio-frequency size effect is observed in fields $H_0 \sim 1$ Oe in bismuth specimens with thicknesses of the order of 10^{-1} cm. We recall that the Fermi surface of bismuth consists of three electron surfaces and one hole surface that are very close to ellipsoidal in shape. The hole ellipsoid is elongated along the trigonal axis C_3, while the major axes of the electron surfaces lie in the planes of symmetry and are inclined 6°23′ to the plane perpendicular to C_3. The electron ellipsoid is strongly prolate. Its maximum dimension exceeds the minimum dimension by a factor of 13.9. The smallest electron cyclotron mass is of the order of $10^{-2}m_e$. More detailed data on the Fermi surface of bismuth can be found in Refs. 41–44, which are reviews devoted specifically to this problem.

The low level of the magnetic field in which the size effect is observed required compensation of the earth's magnetic field. The compensation error was 1%.

In the absence of the high-frequency electromagnetic field, there was no signal from the receiving coil either, since the axes of the low-frequency coils were mutually perpendicular. In accordance with (14), switching on the high-frequency field resulted in the appearance of a direct current in the skin layer and direct-current spikes in the interior of the specimen. As a result, the specimen exhibited a macroscopic magnetic moment whose magnitude and direction were determined by the sum of the fields: $H_0 + H_M \sin\omega_M t$. Generally, the direction of the constant magnetic field did not coincide with the axis of either of the low-frequency coils, and the magnetic field was modulated in both magnitude and direction. Modulation of the field caused changes in the magnitude and direction of the specimen's macroscopic magnetic moment, and these, in turn, set up an induction *emf* in the receiving coil. As a result, the signal registered in the experiment was a mixture of the derivatives of the projection of the specimen's macroscopic magnetic moment M on the receiving-coil axis with respect to the magnitude of the magnetic field and the azimuthal angle.

A typical experimental curve is shown in Fig. 7. For comparison, the same figure shows a record of the linear radio-frequency size effect that was made at a rather low alternating-field amplitude ($H_1 \leq 0.1$ Oe). The

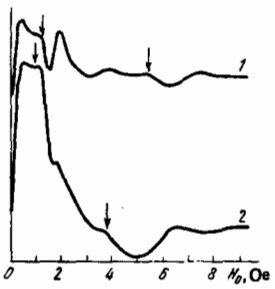

FIG. 7. Traces of radio-frequency size-effect lines (curve 1, $H = 0.1$ Oe) and lines of nonlinear size effect (curve 2). The trigonal axes of the specimen was parallel to the normal to the plane of the plate, $\mathbf{H}_1 \| C_1, \mathbf{H}_0 C_2 = 13°, H_1 = 2.3$ Oe, $d = 0.58$ mm. The arrows mark the origins of the lines. The lines from the two different electron ellipsoids on curve 2 are of different signs.

figure shows that the specimen's macroscopic magnetic moment behaves nonmonotonically approximately at the magnetic-field values at which the lines of the linear size effect occur. It is easily seen that the widths of the linear and nonlinear size-effect lines are practically the same, although the frequencies at which the ω and ω_M records were made differ by factor of $2 \cdot 10^3$. It is this that enables us to state with confidence that changes in the specimen's magnetic field due to direct-current spikes were observed in the experiment.

At certain orientations of the magnetic field with respect to the crystallographic axes of the specimen, we observed a line in the doubled field on the $U(H_0)$ curve (Fig. 8), i.e., a line whose position, reckoned from the left-hand margin, corresponded approximately to satisfaction of the condition $2D = d$. This line was strongest at H_0 directions near the binary C_2 axis. Although the condition $D = 2D$ was satisfied approximately, there is no doubt that the observed line corresponds to emergence of a current spike with $N = 2$ on the opposite side of the specimen. In fact, the size-effect lines from two electron ellipsoids coincide at $\mathbf{H}_0 \| C_2$, while the line of the third is in a much stronger magnetic field.

The shape of the line in the doubled field duplicated the shape in the single field (for which $D = d$), but, in accordance with the calculated prediction, the line in the doubled field was of the opposite sign. As Fig. 7 shows, the lines from different ellipsoids also differed in sign. The sign of a line was determined by the way in which the velocity of the "effective" electrons belonging to the particular ellipsoid were oriented in the

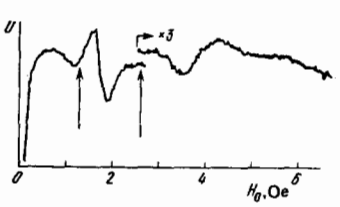

FIG. 8. Nonlinear size effect. Voltage U on receiving coil vs. external magnetic field $\mathbf{H}_0$; $\mathbf{H}_0 \| C_2, C_3$, $\| \mathbf{n}, \mathbf{H}_1 \| C_1, d = 0.58$ mm. The vertical arrows mark the calculated values for the origins of the size-effect lines. The horizontal arrow indicates the point at which the amplification is tripled.

skin layer.[9,45]

In accordance with the theoretical predictions, an increase in the strength of the alternating field resulted in an increase in the amplitude of the observed lines in proportion to H_1^2 up to $H_1 \sim 2$ Oe (Fig. 9). The linewidth increased simultaneously. As would be expected, the lines narrowed when the frequency was increased at a given H_1. Raising the temperature of the helium line resulted in a sharp decrease in the amplitude of the nonlinear size-effect lines, such that they were no longer observed at 4.2 K in specimens 0.6 mm thick.

The shift of the experimentally observed lines from the lines of the linear radio-frequency effect registered at small H_1 is no doubt due to the presence of the magnetic field set up by the rectified current in the interior of the specimen. In principle, the amount of the shift could be used to measure this field. The order of magnitude of the field measured in this way agrees with the estimate obtained from relation (14), although the conditions $H_1 \ll H_0$ and $\Omega\tau \gg 1$ were not satisfied exactly in the experiments. The shift increased with increasing H_1. The linear size effect observed at high radio-wave amplitudes can also be used for direct measurement of the magnetic field created by the rectified current.[46]

On the whole, the experimental results agree quite well with the theory. Certain differences, e.g., departure of the line-amplitude curve from H_1^2, are observed where the theory no longer applies. The only serious disagreement between theory and experiment is the fact that the origin of the size-effect lines for $N = 1$ was in the range in which the magnetic-field vector is parallel to the external magnetic field. [See below for experimental measurement of $M(H_0)$.]

4. "CURRENT" STATES

a) General considerations

It was assumed in the preceding section that the alternating-field amplitude was much smaller than the constant magnetic field in the specimen. We shall now consider the opposite case, in which the constant field is small compared with the amplitude of the alternating field. The skin effect is still anomalous, so that the characteristic dimensions of the electron orbits are much larger than the dimensions of the skin layer. This last condition places an upper bound on the alternating-field amplitude.

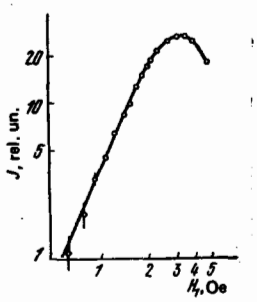

FIG. 9. Amplitude J of lines of nonlinear size effect vs. H_1. $C_3 \| \mathbf{n}$, $\mathbf{H}_0 C_1 = 5°$, $\mathbf{H}_1' \| C_1$.

The electron paths are now strongly distorted in the spatially nonuniform field that is the sum of the wave magnetic field and the constant magnetic field H. Further, the shape of the effective-electron trajectories depends on the mutual orientation of the fields H_1 and H and therefore also on the phase of the wave. The paths are similar to those shown in Fig. 10a during the half-period when H_1 and H are parallel and to those in Fig. 10b in antiparallel fields. The angle at which an effective electron escapes from the skin layer is of the order of $\sqrt{\delta e H_1/mcv}$. While this angle is small $\sqrt{\delta e H_1/mcv} \ll 1$, the electron has different path lengths between two returns to the skin layer in the motions along the paths of Figs. 10a and 10b. The electron sinks into the skin layer more times between two scattering events when the fields H_1 and H are antiparallel than when they are parallel. The magnitude of the current in the skin layer is proportional to the number of effective-electron returns into the skin layer, and for this reason the currents will be different in different half-periods and a rectified current will appear on the surface of the specimen. It flows in the direction opposite to that of the rectified current at $H_1 < H$. The magnetic field of the rectified current changes sign as H increases: it is directed along H in weak fields, where $H_1 < H$, and against H in strong fields.

The above rectification mechanism exists when the effective-electron path length in the skin layer is shorter than the free path, i.e., if the amplitude of the alternating field exceeds the field h_a introduced in paragraph d) of Sec. 2.

The number of returns of the effective electrons into the skin layer is determined by the level of the constant magnetic field outside of the skin layer, where there is now no current. We may therefore conclude that the field H is composed of the external field H_0 and a field $\mathcal{H}$ created by the rectified current itself. In other words, the rectified-current field is a function of the sum of fields $H_0 + \mathcal{H}$: $\mathcal{H} = f(H_0 + \mathcal{H})$. Since the path length between two returns into the skin layer for an effective electron moving along the orbit of Fig. 10a is greater than the free path in weak fields $H < (v/l)mc/e$, we may assume that the number of returns increases with H only in the case corresponding to Fig. 10b. The rectification efficiency and the field of the rectified current are determined by two parameters: the amplitude of

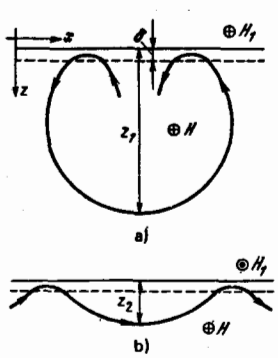

FIG. 10. Paths of effective electrons in different half-periods of alternating field.

the high-frequency wave and the magnitude of the total magnetic field, and the function f increases rapidly with increasing H. If $\partial f/\partial H > 1$, the field $\mathcal{H}$ becomes a nonunique function of the external magnetic field. This is illustrated by Fig. 11. It shows a graphical solution of the equation system

$$\mathcal{H} = f(H), \qquad H = H_0 + \mathcal{H} \tag{15}$$

It is seen from this figure that there is a range of fields at $\partial f/\partial H > 1$, in which several values of $\mathcal{H}$ correspond to a given value of the external magnetic field.

It is easily surmised that the appearance of nonzero values of $\mathcal{H}$ at zero external field H_0 is possible in principle at high alternating-field amplitudes. A graphical solution of Eqs. (15) for $H_0 = 0$ appears in Fig. 12. The dot-dash lines intercept segments on the axis of abscissas that are equal to the fields H_0 at which a jumpwise change in $\mathcal{H}$ occurs within the metal. For there to be nonzero solutions of (15) at $H_0 = 0$, it is necessary that the inequality $f(H_{max}) > H_{max}$ be satisfied; here H_{max} is the field corresponding to the maximum of $f(H)$. In this case, there is a possibility for the metal to acquire a magnetic moment in a zero external magnetic field under radio-frequency irradiation. Such states of a metal with nonzero magnetic moment, which are known as "current" states, have been observed experimentally in bismuth[47,48] and tin.[49]

Metals with complex electron spectra have several groups of effective electrons, which are situated on different areas of the Fermi surface. As we have noted, the contribution of electrons of a given group to the rectified current depends on the projection of their velocity in the skin layer onto the direction of the high-frequency current and on the number of times that they return into the skin layer during the interval between collisions. The latter is determined not only by the magnitude, but also by the direction of the magnetic field in the interior of the metal; in such metals, therefore, the direction of the rectified current may not, in the general case, coincide with that of the high-frequency current. This means that there may be "current" states corresponding to different directions of the specimen's magnetic moment when several groups of effective electrons are present.

The presence of "current" states results in hysteretic behavior of all properties of the metal that depend on the magnetic field in the interior of the specimen. In metals with complex Fermi surfaces, a change in the contributions of one of the electron groups to rectification influences the efficiency of rectification by other electron groups. As a consequence, the widths and positions of the hysteresis loops may come to depend in rather complex fashion on the direction of the external magnetic field. In particular, hysteresis loops may appear in comparatively strong magnetic fields. Such loops have been observed experimentally in bismuth.[47,48]

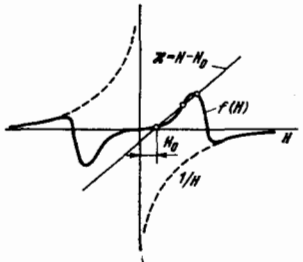

FIG. 11. Graphical solution of equation system (15). The open circles represent possible states in the external field H_0.

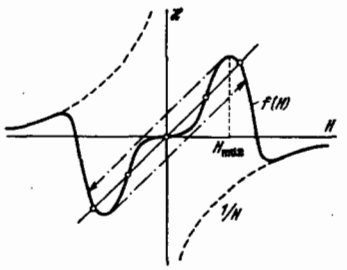

FIG. 12. Graphical solution of system (15) in the case in which states with nonzero magnetic moment are possible in a zero external magnetic field.

We stress that, in contrast to the hysteresis phenomena observed in ferromagnetics, the transition from one value of the specimen's magnetic moment to another in the presence of "current" states does not take place gradually, but is abrupt, occurring at definite values of the external magnetic field.

b) Calculation of rectified current

To satisfy ourselves that "current" states may appear, we must compute the shape of the $\mathcal{H}(H)$ curve in a weak magnetic field H. For the calculation, we shall use an elementary Fermi-surface model in the form of a cylinder with its axis in the y direction and assume that the fields are oriented as shown in Fig. 10.

It is now inconvenient to use successive approximations to find the magnitude of the rectified current, since the current is governed by qualitative changes in the form of the electron orbits. We shall make use of the quasistatic property of the fields E_1 and H_1 to find the current. At given E_1 and H_1, the electric current density is determined[50] by the expression

$$j_x = (1 - e^{-T/\tau})^{-1} \left\langle e^2 v_x \int_{t-T}^{t} e^{(t'-t)/\tau} v(t') E\left(z + \int_{t}^{t'} v_z(t_1)\, dt_1\right) dt' \right\rangle, \tag{16}$$

where the angle brackets signify averaging over the Fermi surface. The dependence of current density on magnetic field is concentrated in the first cofactor of (16).[50] Therefore the total current flowing through the skin layer is

$$J = \int_0^\infty j(z)\, dz \sim (1 - e^{-T/\tau})^{-1} \int_0^\infty j_0(z)\, dz, \tag{17}$$

where j_0 is the current density in the absence of a magnetic field. Strictly speaking, the conversion from (16) to (17) is valid only in the case of a uniform magnetic field. If this field is nonuniform, the period T of the electrons' motion becomes a function of z and of the position of the electron on the Fermi surface. In our case the magnetic field is composed of a constant field and the wave field H_1, and is spatially nonuniform as a

result. Nevertheless, we shall use expression (17) for approximate calculations, bearing in mind that the main contribution to conductivity comes from "effective" electrons for which T depends quite weakly on z. For T we shall use the period of motion of the electrons that move parallel to the surface at $z=0$. As a result of this simplification, all of the calculations that follow become qualitative in nature.

To find the value of the rectified current, it is sufficient to average (17) over the period of the alternating field. We then obtain for the field $\mathcal{H}$

$$\mathcal{H} = \frac{H_1}{2\pi}\int_{\varphi_1}^{\varphi_2} \sin\left(\varphi - \frac{\pi}{6}\right)(e^{T(\varphi)/\tau}-1)^{-1}\,d\varphi = f(H_1, \mathcal{H}), \qquad (18)$$

which recognizes that the path of Fig. 10b, which is responsible for the appearance of "current" states, exists while $\int_0^\infty H_1(z)dz = H_1(0)\delta\sin\varphi > H\delta$, i.e., as long as the phase φ lies in the range

$$\varphi_1 = \arcsin\frac{H}{H_1} \leqslant \varphi \leqslant \pi - \arcsin\frac{H}{H_1} = \varphi_2. \qquad (19)$$

Relation (18) also omits returns of electrons into the skin layer along the path of Fig. 10a ($\tau eH/mc \ll 1$) and neglects the dependence of the metal's surface impedance on the field of the electromagnetic wave. The latter is possible at $\mathcal{H}/H_1 \ll 1$, since the relative correction to the impedance is of the order of $\mathcal{H}/H_1$.

To calculate $\mathcal{H}$, it remained to determine the period of effective-electron motion. We note that the vector potential of the magnetic field, which depends only on the z coordinate and is directed along the y axis, can be represented in the form

$$A_x = \int_0^z H(z)\,dz \qquad A_x = A_y = 0.$$

For this form of the vector potential, the electron Hamiltonian does not contain the x coordinate, and the projection of the generalized momentum onto the axis is preserved:

$$p_x + \frac{e}{c}A_x = \text{const}. \qquad (20)$$

We are interested in the motion of electrons whose velocities are parallel to the surface at $z=0$, i.e., those for which the momentum equals $p_x = \sqrt{2m\varepsilon_F}$, $p_z = 0$ at $A_x = 0$. The magnetic field does not perform work on a charged particle,[51] so that the kinetic energy of the electron is also conserved:

$$(2m)^{-1}(p_x^2 + p_z^2) = \varepsilon_{ph}. \qquad (21)$$

With (20), the energy conservation law can be rewritten

$$(2m)^{-1}\left[p_z^2 + \left(\sqrt{2m\varepsilon_{ph}} - \frac{e}{c}A(z)\right)^2\right] = \varepsilon_{ph}. \qquad (22)$$

This equation shows that the motion of an electron along the z coordinate is similar to the motion of a particle that possesses an energy ε_F in a one-dimensional potential well with potential $\Pi(z) = (2m)^{-1}[\sqrt{2m\varepsilon_F} - e/cA(z)]^2$. According to Ref. 52, the period of this motion is determined by the expression

$$T(\varepsilon_{ph}) = \sqrt{2m}\int_{z_0}^{z_1}\frac{dz}{\sqrt{\varepsilon_{ph}-\Pi(z)}}, \qquad (23)$$

where the $z_{0,1}$ are the turning points of the electron, which are roots of the equation $\varepsilon_F = \Pi(z)$. The vector potential is so chosen that $z_0 = 0$.

The period is easy to calculate if we assume that the field decreases exponentially in the thin layer, the electron's angle of escape from the skin layer is small, $\sqrt{eH_1\delta/mvc} \ll 1$, and $H_1 \gg H$. Given these conditions, the period equals

$$T(\varphi) = \tau h_a^{1/2}[(H_1\sin\varphi)^{-1/2} + (H_1\sin\varphi)^{1/2}H^{-1}] \qquad (24)$$

for the case of antiparallel H_1 and H. If $H_1 \sim H$, expression (24) is of the nature of an estimate. We note that the period of electron motion has distinct structure. The first term in the square brackets refers to the time after which the electron will be ejected from the skin layer by the field H_1, and the second term to the time after which it will return under the action of the field H.

Figure 13 shows curves of $\mathcal{H}(H)$ obtained from (18), (19), and (24) for various values of the alternating-field amplitude, and Fig. 14 the analogous curves for the derivative $\partial\mathcal{H}/\partial H$. The specimen has states with nonzero magnetic moment in a zero magnetic field even at $H_1 \sim 50h_a$. According to Fig. 14, the hysteresis loop that appears at $\partial\mathcal{H}/\partial H \geqslant 1$ exists in an even weaker alternating field, $H_1 \gtrsim 30h_a$.

Let us now formulate the principal features of the phenomenon that do not depend on the model used for the calculation and can be verified easily in experiment:

1. Threshold nature. The appearance of hysteresis loops can be expected only after the amplitude of the alternating field has reached a certain critical value H_1^c.

2. Stepwise transition from one state to another. Since the transition time is determined by the damping of Foucault currents in the specimen, this time will be longer in thick specimens and in metals with higher conductivity.

3. The existence of a characteristic scale of the fields h_a. Since the critical amplitude H_1^c is proportional to h_a, we have $H_1^c \sim \delta$. If the skin-layer depth itself does not depend on the alternating-field amplitude, then $H_1^c \sim \omega^{-1/3}$.

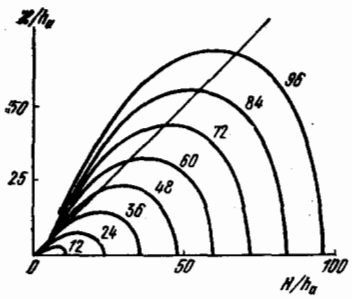

FIG. 13. Theoretical curves of field $\mathcal{H}$ vs. constant magnetic field in interior of specimen. The amplitude of the alternating field in units of h_a is indicated beside each curve.

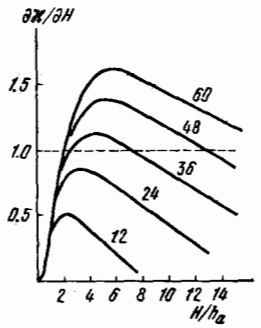

FIG. 14. The derivative $\partial\mathcal{H}/\partial H(H)$. The numbers beside the curves are values of H_1/h_a.

c) Experimental observation of "current" states in bismuth

"Current" states can be studied with the same system of three induction coils that was used in the case of the nonlinear size effect (see Fig. 6). The simplest observing procedure is to vary the external magnetic field in accordance with the law $H_0 = H_M \sin\omega_M t$ and follow the signal from either of the receiving coils 4 or 5. Since the magnetic field H_0 in the interior of the specimen must be uniform, the modulation frequency is low, $\omega_M \lesssim 100$ Hz. The modulation amplitude H_M may range up to several oersteds. Since the signal from the receiving coil is proportional to $\partial M/\partial t$, where M is the projection of the specimen's magnetic moment onto the axis of the coil, we should expect the appearance of sharp overshoots of the recieved signal on stepwise changes in the magnetic moment of the specimen. Generally, both the magnitude and direction of the magnetic moment will change, so that either of the coils 4 or 5 can be used as the receiving coil.

The results of such experiments on a bismuth specimen are shown in Figs. 15 and 16. In the simplest case (Fig. 15), signal spikes are observed on only one of the receiving coils. There are two distinct spikes corresponding to magnetic-moment reversal. In the more complex situation (Fig. 16), the signals from the receiving coils are similar but they have more complex structure.

The time after which the magnetic moment of the specimen will change can be estimated easily from the widths of the spikes shown in Figs. 15 and 16. The order of magnitude of this time is 10^{-3} sec, which is quite consistent with the decay time of eddy currents in bismuth.

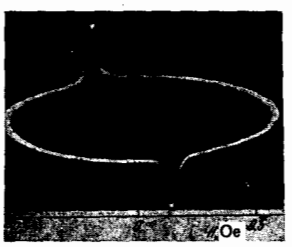

FIG. 15. Photograph from oscilloscope. Signal from receiving induction coil whose axis coincides with the direction H_1; $d = 0.4$ mm, $C_3 \| \mathbf{n}$, $\mathbf{j}_1\mathbf{C}_1 = 4°$, $\mathbf{j}_1\mathbf{H}_0 = 95°$, $H_1 = 22$ Oe, $\omega_M/2\pi = 76$ Hz. Note the jumpwise changes in the magnetic moment of the bismuth specimen.

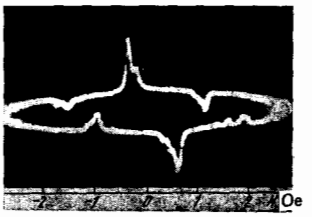

FIG. 16. Magnetic-moment jumps in bismuth specimen at $H_1 = 15$ Oe, $\omega_M/2\pi = 37$ Hz, $d = 0.4$ mm, $\mathbf{j}_1\mathbf{H}_0 = 24°$.

Using photographs taken from the oscilloscope, we can estimate the magnetic field $\mathcal{H}$ created by rectification of the high-frequency current. To this end, it is necessary to compare the signal that arises from sinusoidal variation of the external magnetic field $H_0 = H_M \sin\omega_M t$ with the signal corresponding to reversal of the specimen's magnetic moment. When the parameters of Fig. 15 are used, this comparison gives[48]: $\mathcal{H} = 0.7-1.4$ Oe. The large error results from the fact that a not very accurately known part of the magnetic flux set up by the rectified current is closed inside the receiving coil.

It is convenient to use a modulation procedure, recording curves of $\partial M/\partial H_1(H_0)$, to obtain more accurate measurements of the dimensions of the hysteresis loops. For this purpose, it is sufficient to modulate the amplitude of the alternating field with a frequency ω_M and register the magnetic-field dependence of the low-frequency component of the signal from the receiving coils. In principle, any quantity that depends on the specimen's magnetic moment can be used for measurements. In the first experiments,[47] for example, the derivatives of the specimen's surface impedance were recorded.

Figure 17 shows typical $\partial M/\partial H_1(H_0)$, curves for bismuth specimens with the trigonal axis directed along the normal [to] the plane of the plate. The presence of several states is observed in two magnetic-field ranges, whose extent is indicated on the figure by arrows A and B. One of the ranges brackets the point $H_0 = 0$. An in-

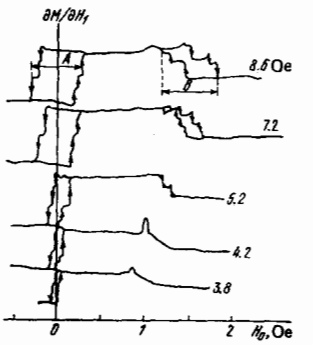

FIG. 17. Curves of $\partial M/\partial H_1(H_0)$ at various alternating-field amplitudes. Receiving-coil axis parallel to H_1, $d = 0.4$ mm, $\mathbf{j}_1\mathbf{H}_0 = 15°$, $\mathbf{j}_1\mathbf{C}_1 = -4°$. The amplitude of H_1 is indicated beside each curve.

crease in the amplitude of the electromagnetic field broadens this range, and the initial segment of the $A(H_1)$ curve is nearly linear (Fig. 18). H_1^c can be obtained by extrapolating the linear relation to zero hysteresis-loop size. For most specimens, the smallest value of H_1^c at 1.3 K was approximately 4 Oe. H_1^c increases with temperature. For bismuth, the H_1^c obtained by extrapolating the $A(H_1)$ line depends on the direction of the external magnetic field when the hysteresis loop was recorded: H_1^c is smallest when $\mathbf{H}_0 \perp \mathbf{j}_1$ and largest when $\mathbf{H}_0 \| \mathbf{j}_1$.[47]

Figure 19 shows how the dimension A depends on the direction of the external magnetic field. The angular interval over which the currents are recorded is smaller than π because the two ranges in which several states exist are superimposed on one another at small angles between the high-frequency current and the magnetic field. The figure shows that dimension A increases as the vector of H_0 approaches the direction of the high-frequency currents.

The second range in which several states exist appears at H_1 larger than the range bracketing the coordinate origin (see Fig. 17). A singularity forms on the $\partial M/\partial H_1(H_0)$ curve even before it appears. Increasing the amplitude of the alternating field increases the size of this singularity and moves it away from the origin. In the range around the origin, the magnetic moment of the specimen increases if the magnetic field increases and decreases on a decrease in the magnetic field, while the signs of $\partial H_0/\partial t$ and $\partial M/\partial t$ are reversed in the second range.

In specimens with the C_3 axis near the normal, the second range is observed only when the magnetic field lies inside a 60° range of angles between the binary axes that form the smallest angles with the direction of the high-frequency currents (Fig. 20). When the specimen is rotated within the measuring-coil system, the position of this sixty-degree interval also changes.

The question arises as to whether the apperance of the second hysteresis loop can be understood, and the width and position variation of the loops with angle interpreted, within the framework of the model used for calculation previously. To answer this question, it will be necessary to perform a calculation using a more realistic Fermi-surface model and consider the reciprocal effects among the various electron groups. Following Ref. 53, we shall use a model of the electronic part of the Fermi surface of bismuth that consists of three cylindrical surfaces. Neglecting the six-degree inclination, we shall assume that the axes of

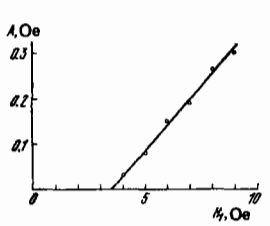

FIG. 18. Width A of hysteresis loop vs. H_1. $d = 0.4$ mm, $\mathbf{j}_1 C_1 = 2°$, $\mathbf{j}_1 \mathbf{H}_0 = 95°$, $T = 1.3$ K.

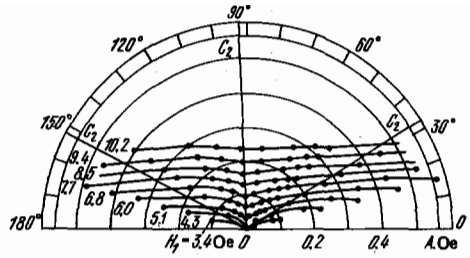

FIG. 19. Dimension A vs. direction of external magnetic field (polar coordinates). The direction of the high-frequency currents was used as the reference origin; $d = 0.4$ mm, $\mathbf{j}_1 C_1 = 2°$.

the cylinders lie in the same plane and that the angle between axes is 120°. In accordance with experimental conditions, we direct the high-frequency current along the axis of one of the cylinders. Then electrons of this cylinder will make no contribution at all to the current (the velocity of the electrons is perpendicular to the direction of the current), and the contributions from the other two cylinders will be equal and depend weakly on H_0 as long as $eH\tau/mc \lesssim 1$. Let us denote by $\mathcal{H}_1$ and $\mathcal{H}_2$ the constant fields that arise as a result of variation of the electron paths of different cylinders. These fields, directed along the axes of the cylinders, can be found from the equation system

$$\begin{aligned} \mathcal{H}_1 &= \beta f\left(H_1\frac{\sqrt{3}}{2},\ H_0\cos\left(\frac{\pi}{3}-\psi\right)\right. \\ &\qquad \left. +\mathcal{H}_1-\frac{\mathcal{H}_2}{2}\right), \\ \mathcal{H}_2 &= \beta f\left(H_1\frac{\sqrt{3}}{2},\ H_0\cos\left(\frac{\pi}{3}+\psi\right)\right. \\ &\qquad \left. +\mathcal{H}_2-\frac{\mathcal{H}_1}{2}\right); \end{aligned} \tag{25}$$

here f is a function that states the relation between $\mathcal{H}$ and H in accordance with (18) in the case of one cylinder and the angle ψ is reckoned from the direction of the high-frequency current. The coefficient β takes account of the hole contribution to the high-frequency conductuvity. ($\beta = 2/3$ if the hole contribution is neglected.)

The results of numerical solution of Eqs. (25) were reported in Ref. 53. The width of the hysteresis loop

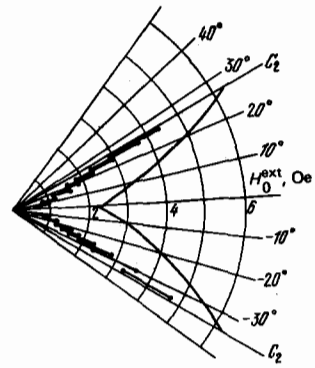

FIG. 20. Position of range E vs. direction of constant magnetic field. The length of a bar indicates the width of region B; $d = 0.4$ mm, $H_1 = 7.2$ Oe. The solid curve represents the calculation with formulas (27); $h_a = 0.06$ Oe, which corresponds to $\delta = 2 \cdot 10^{-3}$ cm, $\tau = 5 \cdot 10^{-10}$ sec, and $\beta = 2/3$.

around the origin was determined as a function of external magnetic field direction. The form of the calculated curves agrees only qualitatively with the experimental relationships. Considering the many simplifying assumptions made for the calculation, it would be difficult to expect anything better.

The appearance of the second hysteresis loop is easily explained when it is remembered that the projection of the resultant field $H = H_0 + \mathcal{H}_1 + \mathcal{H}_2$ onto the axis of one of the electron ellipsoids can change sign in a comparatively large external magnetic field H_0^{ext}. Substituting a cylindrical surface for the ellipsoidal Fermi surface, we may treat the number of electron returns into the skin layer as dependent only on the projection of the resultant magnetic field onto the cylinder axis; therefore the field H_0^{ext} is indistinguishable from the zero field for electrons on one of the cylinders.

We find the field H_0^{ext} by putting $\mathcal{H}_2 = 0$ in (25):

$$\mathcal{H}_1 = 2H_0^{ext}\cos\left(\frac{\pi}{3}+\psi\right),$$
$$\mathcal{H}_1 = \beta f\left(H_1\frac{\sqrt{3}}{2},\ H_0^{ext}\cos\left(\frac{\pi}{3}-\psi\right)+\mathcal{H}_1\right). \qquad (26)$$

Figure 20 shows the result of calculations using formulas (26) without the hole contribution to the high-frequency conductivity. The calculated value average twice the experimental value.

The quantity β could have been used as a free parameter to fit the calculation to the experiment. A different problem was posed in Ref. 53: construct the function $f(H_0)$ from a $H_0^{ext}(\psi)$ relation known from experiment in accordance with the first equation of (26). The relation

$$\mathcal{H}(H_0) = 2\beta f\left(H_1\cdot\frac{\sqrt{3}}{2},\ H_0\cdot\frac{1\sqrt{3}}{2}+\mathcal{H}\cdot\frac{\sqrt{3}}{2}\right)$$

plotted from the experimental points corresponding to Fig. 20 is shown in Fig. 21. Also included as a solid curve is a relation obtained experimentally by a different, independent method. It was plotted from records of $H_1\partial\mathcal{K}/\partial H_1(H_0)$ curves corresponding to various alternating-field amplitudes. (A signal proportional to $H_1\partial\mathcal{K}/\partial H_1$ appears at the receiving induction coil on shallow low-frequency modulation of the alternating field if the specimen's magnetization changes only in magnitude and not in direction on a change in H_0. This last condition is satisfied if $H_0 \perp j_1 \| C_1$.) With the set of

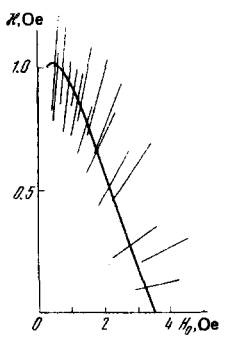

FIG. 21. $\mathcal{H}(H_0)$ plotted from results of two independent experiments: $C\|n, d = 0.4$ mm, $j_1 | C_1, H_1 = 7.2$ Oe.

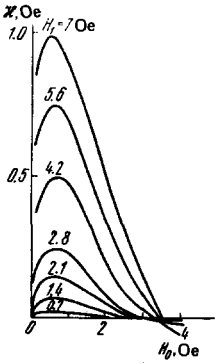

FIG. 22. Rectified-current field vs. external magnetic field at various H_1.

curves proportional to $H_1\partial\mathcal{K}/\partial H_1$, the dependence $\mathcal{K}(H_0)$ can be found by numerical integration, though with accuracy only to an unknown numerical multiplier. As Fig. 21 shows, the curve found in this way can be fitted within the limits of error to the points obtained from the angular variation of the position of the hysteresis loop. This, first, justifies the assumption and, second, provides a calibration coefficient. The error of calibration is about 10%. Figure 22 shows $\mathcal{K}(H_0)$ plots for several alternating-field amplitudes as constructed with the calibration coefficient found in this way. In accordance with the considerations advanced in paragraph a) of Sec. 4, the field $\mathcal{K}$ changes sign as H_0 increases.

One of the experimental results obtained on bismuth[48] was unexpected. It was found that neither H_1^c nor the width $A(H_1)$ of the hysteresis loop depended on frequency at a constant H_1. The absence of any noticeable frequency dependence was verified[49] in a broad frequency range from $275\cdot10^3$ to $5\cdot10^6$ Hz. The depth of the skin layer in specimens of the same quality varied in proportion to $\omega^{-1/3}$ in the same frequency range.[54] It is possible that the absence of frequency dependence is due to the effect of the alternating-field amplitude on the surface impedance of the specimen, which itself may be different at different frequencies. Nor is a certain asymmetry of the $\partial M/\partial H_1(H_0)$ curves fully understood. This asymmetry is noticeable in Fig. 17: stepwise changes in the magnetic moment are observed at various values of the magnetic field, depending on the direction from which the external field H_0 approaches zero.

d) Experiments on tin

Tin has a much more complex Fermi surface than bismuth, and its number of conduction electrons is typical for a metal, i.e., it exceeds the number of conduction electrons in bismuth by five orders of magnitude. Therefore experiments on tin can be regarded as a test verifying that media with different conductivities have the phenomenon in common.

In the simplest model with isotropic square-law dispersion, H_1^c depends very weakly on the conduction-electron concentration, $H_1^c \sim H_a \sim n^{1/9}$. The power released in the specimen when the alternating field reaches its critical value, $w \sim \delta(H_1^c)^2$, does not depend

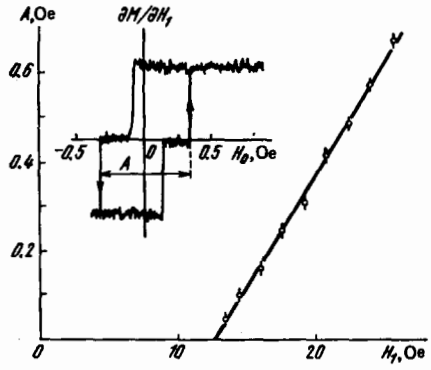

FIG. 23. Width of hysteresis loop in tin as a function of alternating-field amplitude. $\mathbf{n}\|[001]$, $d=0.6$ mm, $T=4.15$ K, $\mathbf{H}_0\|[100]$, $\mathbf{H}_0\mathbf{H}_1=10°$, $\omega/2\pi=1.7$ MHz. Record of $\partial M/\partial H_1$ is shown at $H_1=25.5$ Oe.

on conduction-electron concentration at all.

The results obtained on tin plates with the fourth-order axis along the normal are generally the same as the experimental results obtained on bismuth. At high alternating-field amplitudes, characteristic hysteresis loops are observed on the $\partial M/\partial H_1(H_0)$ curves (Fig. 23). The loop dimension A increases linearly with increasing H_1. Figure 24 shows how the loop width depends on the direction of the external magnetic field relative to the crystallographic axes. The relation represented in this figure corresponds to polarization of the high-frequency currents along the [100] direction. A change in the polarization of the high-frequency currents by angles ±15° does not affect the manner in which the width of the loop varies with the direction of the external magnetic field. In contrast with the case of bismuth, the critical alternating-field value found by extrapolating the $A(H_1)$ line to zero hysteresis-loop size did not depend on the direction of the constant magnetic field at which the hysteresis loop was recorded. Another difference was that variation of the frequency influenced H_1^c in tin (Fig. 25). The positions of the plotted points are described by an ω^{-k} curve with $k=0.38\pm0.05$. Therefore the results obtained for tin are not at variance with the $H_1^c\sim\omega^{-1/3}$ relation predicted by the theory. We note that changing the frequency in the range studied had no influence on the slopes of the $A(H_1)$ curves.

In specimens with the [001] axis along the normal (see Fig. 24), the width of the hysteresis loop depended on angle as though the main contribution to rectification came from a cylindrical area of the Fermi surface. Such areas are indeed observed in zones 4 and 5 in the case of tin.[55] As Fig. 26 shows, a similar angular dependence is also observed on specimens with the [110] axis along the normal. If the high-frequency current is directed along $[\bar{1}10]$, the initial segment of the $A(H_1)$ curve is linear (Fig. 27), but the linear dependence breaks at a certain alternating-field amplitude corresponding to the inflection point on the $A(H_1)$ curves does not depend on the direction of the magnetic field during measurement of this curve. The appearance of the break is evidently due to the appearance of another group of electrons that move along an orbit of the type shown in Fig. 10b at amplitudes exceeding the alternating-field amplitude corresponding to the break. If the high-frequency current is polarized along [001], two separate hysteresis loops appear symmetrically disposed about the origin at small H_1. As H_1 increases further, they merge to form a single loop that brackets the point $H_0=0$. Figure 26 shows the variation of the distance between the centers of these loops (see inset in Fig. 26) as a function of the direction of the constant magnetic field. Again in this case, it appears from the angular variation that the main contribution to rectification is associated with electrons of cylindrical areas of the Fermi surface.

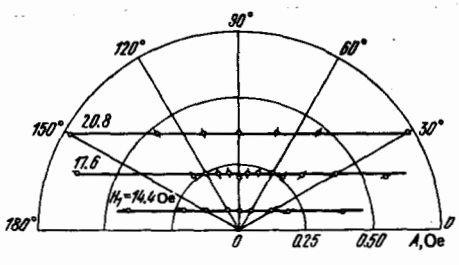

FIG. 24. Dimension A vs. direction of external magnetic field. Tin, $d=0.6$ mm, $T=4.15$ K, $\mathbf{H}_1\|[100]$, $\mathbf{n}\|[001]$.

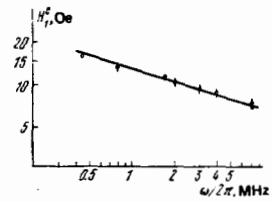

FIG. 25. H_1^c vs. frequency of alternating field in tin. The straight line corresponds to $H_1^c\sim\omega^{-1/3}$.

In the tin specimens, the magnetic moment was reversed in about 10^{-2} sec. This is several times longer than the times for bismuth.

In the aggregate, the data obtained for tin indicate that the "current" states in this metal owe their origin not to electrons of small closed fragments of the Fermi surface, as in bismuth, but to modification of the elec-

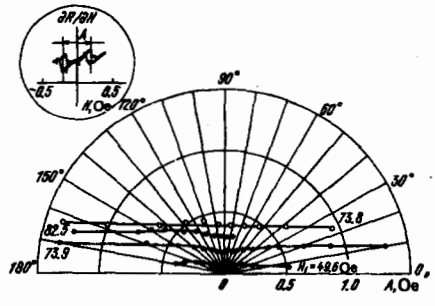

FIG. 26. Dimension A at various external magnetic field directions. Tin, $d=0.4$ mm, $\mathbf{n}\|[110]$, $T=3.75$ K; the dark circles correspond to the case $\mathbf{j}_1\|[\bar{1}10]$, the open circles to $\mathbf{j}_1\|[001]$. The dimension A for the latter case is indicated in the inset. Angles are reckoned from the direction of the high-frequency field.

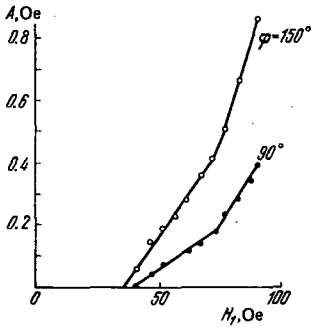

FIG. 27. Width of hysteresis loop vs. alternating-field amplitude. Tin, $d = 0.4$ mm, $\mathbf{n} \| [110], \mathbf{j}_1 \| [-110], T = 3.75$ K, angles measured from direction of high-frequency current.

tron paths on large areas of the Fermi surface by the wave field.

5. SELF-OSCILLATIONS

a) Stability of "current" states

Let us turn now to the stability of various "current" states.[53] As we showed earlier [paragraph b) of Sec. 4], there are, even in the case of the simplest cylindrical Fermi surface in a zero magnetic field, not two but four possible states with nonzero magnetic moment. The derivative $\partial\mathcal{H}/\partial H > 1$ in two of them. Such states have never been observed experimentally. It will be shown below that they are unstable with respect to longwave perturbations of the magnetic field.

The calculations performed in paragraph b) of Sec. 4 did not consider the returns of electrons to the skin layer on large orbits. Allowance for these electrons cannot appreciably change the magnitude of the field $\mathcal{H}$, but it turns out to be significant when we study the stability of "current" states. In fact, the rectified current depends in this case on the values of the magnetic field at the two characteristic points marked z_1 and z_2 in Fig. 10. One of them is at a distance from the surface approximately equal to the diameter of the Larmor orbit, while the other is the characteristic dimension of the nonclosed orbit that appears when the direction of the alternating magnetic field is opposite to that of the constant field.

A change of the magnetic field at either of these points makes itself evident almost instantly in the rectification efficiency, after times of the order of the relaxation time of the electrons, $\tau \ll \omega^{-1}$. However, the change in the rectified current affects the field at points $z_{1,2}$ after times of the order of $\tau_{1,2} \sim \sigma z_{1,2}^3/c^2 r$, which are much larger than τ and differ sharply from one another: $\tau_1 \gg \tau_2$. Under these conditions we may expect the appearance of self-oscillations of the rectified current, and, at the same time, of the specimen's magnetic moment, at the frequencies $\tilde{\omega}$ at which the phase difference is large, $\tilde{\omega}(\tau_1 - \tau_2) \gg 1$, and any phase relation may hold.

Let us first consider the stability with respect to longwave perturbations of the magnetic field. We shall assume that returns of electrons to the skin layer on large orbits can be neglected for either of the following reasons: the total magnetic field H in the interior of the specimen is weak, $l/z_1 \ll 1$, or the specimen itself, which has the form of a plate of thickness 2d, is thin: $(H_1/H)\delta \ll d \ll vmc/eH \approx z_1$.

Assume that an inhomogeneous increment $\delta\mathcal{H}$ to the field $\mathcal{H}$ arises in a specimen that occupies the region $|z| \leq d$ and possesses a magnetic moment as a result of rectification, and that the field $\delta\mathcal{H}$ varies weakly on distances of the order of the characteristic electron-path dimension z_2. We find $\delta\mathcal{H}$ as a function of time. To simplify, we shall again use the cylindrical Fermi-surface model.

The change in the period of motion of the effective electrons as a result of the magnetic-field perturbation will, according to (23), be

$$\delta T = -\frac{\partial}{\partial \varepsilon_{ph}} \sqrt{2m} \int_{z_0}^{z_2} dz \delta\Pi (\varepsilon_{ph} - \Pi_0(z))^{-1/2}, \tag{27}$$

[the perturbing field $\delta\mathcal{H}$ is not present in $\Pi_0(z)$]. The variations with respect to the limits of integration in (27) vanish because

$$\frac{\partial}{\partial \varepsilon_{ph}} \sqrt{\varepsilon_{ph} - \Pi_0(z)} \,|_{z_2} \delta z_2 = 0.$$

Assuming that the dependence on time is determined by the multiplier $e^{i\tilde{\omega}t}$ and that the conditions of the normal skin effect are satisfied for $\delta\mathcal{H}$, we obtain

$$\delta\mathcal{H} = \delta\mathcal{H}(d) \frac{\operatorname{ch} kz}{\operatorname{ch} kd}, \tag{28}$$

where $c^2k^2/4\pi\sigma = i\tilde{\omega}$.

The expansion $\delta\mathcal{H} \approx \delta\mathcal{H}(d)(1 + kz \operatorname{th} kd)$ can be used at distances of the order of z_2 from the surface of the specimen. Then

$$\delta T \approx \frac{\partial T}{\partial H} \delta\mathcal{H}(d) + \alpha k z_2 \delta\mathcal{H}(d) \operatorname{th} kd; \tag{29}$$

here $\partial T/\partial H < 0$ and α is a positive number. Let us calculate the change in the rectified current J due to the magnetic-field perturbation. Since we shall be interested only in the initial segment of the $J(H)$ curve, we put $\varphi_1 = 0$ and $\varphi_2 = \pi$ in (19) and apply Eq. (29):

$$\delta J = \frac{c}{4\pi} [f' \delta\mathcal{H}(d) - bkz_2 \delta\mathcal{H}(d) \operatorname{th}(kd)], \quad b > 0. \tag{30}$$

As would be expected, the change in the rectified current is determined by the value of the magnetic field at point z_2. The current δJ creates a magnetic field $\delta\mathcal{H}^2(d - \delta) \approx \delta\mathcal{H}(d)$ at the point $z = (d - \delta)$, so that $\delta\mathcal{H}(d) = [f' - bkz_2 \operatorname{th}(kd)]\delta\mathcal{H}(d)$, or

$$(f' - 1) b^{-1} \frac{d}{z_2} = kd \operatorname{th}(kd). \tag{31}$$

Figure 28 shows the graphical solution of (31). We

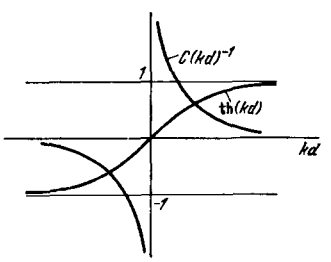

FIG. 28. Graphical solution of Eq. (31) for real K. It is seen that solutions exist for $C = (f' - 1)b^{-1}d/z_2 > 0$.

see from the figure that this equation has roots at real k for $f'>1$. These solutions increase exponentially with time, which corresponds to the appearance of instability. There is, in addition, an infinite set of solutions for purely imaginary k that exists both for $f'>1$ and for $f'<1$. These solutions damp with time, in full agreement with the solutions for ordinary Foucault currents.

Thus, in the case under consideration, only the states in which $f'<1$ will be stable. It is therefore no surprise that states with $f'>1$ have not been observed in experiment. Where it is necessary to take account of electron returns into the skin layer on a large orbit, states with any f' except those in the narrow ranges $1-\sqrt{z_2/z_1}\leq f\leq 1$ are found to be stable with respect to longwave magnetic-field perturbations. However, as will be shown below, the specimen is unstable with respect to the appearance of magnetic-moment self-oscillations at $f'>1$ under these conditions.

b) Growing magnetic-moment oscillations

Self-oscillations are possible in, for example, systems that acquire energy from an external high-frequency-field source. A similar conclusion follows from the work Gurevich and Ioffe,[27] who analyzed the case of a weakly damped energy flux. The contrary case arises in a metal with the anomalous skin effect: the wave damps at distances that are small compared with the dimensions of the specimen. Nevertheless, both the conductivity at the fundamental frequency ω and the nonlinear properties are sensitive to variation of the magnetic field in the interior of the metal because of the long electron free path.

Let us now turn to perturbations at frequencies $\tilde{\omega}$ at which the skin effect is anomalous. Since it is assumed that all possible solutions are damped at a distance $k^{-1}\ll d$, we shall confine ourselves to the case in which the specimen occupies the half-space $z>0$. We shall assume satisfaction of the conditions $z_1\gg k^{-1}\gg z_2$, which make it easy to calculate the change in the periods of electron motion due to an inhomogeneous magnetic-field perturbation $\delta\mathcal{H}$. Under these conditions, the contributions to the rectified current from large orbits that penetrate to depth $z_1\sim 2r$ and orbits that creep along the surface (Fig. 10b) are substantially different in nature. The contribution from orbits of the latter type corresponds to formula (30) as $kd\to\infty$:

$$\delta J_2=\left(\frac{4\pi}{c}\right)^{-1}[f'-bkz_2]\,\delta\mathcal{H}(0). \tag{32}$$

To consider the contribution of orbits of the first type, it is necessary to calculate the change of the corresponding period T in a strongly inhomogeneous magnetic field.

The influence of the alternating field of frequency ω on the period of the motion can be neglected in the calculations. Substituting into (27)

$$\delta\Pi=m^{-1}\left(\sqrt{2m\varepsilon_{\rm ph}}-\frac{e}{c}zH\right)\frac{e}{c}\frac{\delta\mathcal{H}(0)}{k}(1-e^{-kz}),$$

which corresponds to a magnetic-field perturbation $\delta\mathcal{H}=\delta\mathcal{H}(0)e^{-kz}$, $\mathrm{Re}\,k>0$, and evaluating the integral of (27) within the limits 0 and z_1, we obtain

$$\frac{\delta T}{T}\sim-\frac{\delta\mathcal{H}}{\mathcal{H}}e^{-kz_1}[I_0(kz_1)-I_1(kz_1)]. \tag{33}$$

The corresponding contribution to the rectified current will therefore be $\delta J_1=-\delta\mathcal{H}(0)(4\pi/c)^{-1}a(kz_1)^{-3/2}$, where a is a positive number of the order of $(z_2/z_1)^{1/2}$. The minus sign indicates than an increase in the number of returns during the half-period under consideration lowers the rectified current. Since $\delta\mathcal{H}(0)=4\pi/c(\delta J_1+\delta J_2)$, we have

$$1=f'-bkz_2-a\,(kz_1)^{-3/2}. \tag{34}$$

Since the nature of the spatial inhomogeneity corresponds to anomalous skin-effect conditions, the time dependence is determined by the multiplier $e^{i\tilde{\omega}t}$, where $\tilde{\omega}$ satisfies the condition

$$\tilde{\omega}=-\frac{c^2k^2r}{3\pi^2\sigma}, \tag{35}$$

and k must be found from (34). Here we have used an approximate expression for the effective conductivity in a strong magnetic field. Although this expression is not valid in the case of a cylindrical Fermi surface,[37] its use can be justified by the fact that real metals have cylindrical Fermi-surface areas that contribute significantly to the shaping of skin-layer structure.

Let us introduce the new variable $kz_1=\rho^{i\varphi}$, where $0<\varphi<\pi/2$, and the quantity $\tilde{b}=bz_2/z_1$. Separating the real and imaginary parts in Eq. (34), we obtain

$$\tilde{b}\rho\sin\varphi-a\rho^{-3/2}\sin\frac{3\varphi}{2}=0, \tag{36}$$

$$\tilde{b}\rho\cos\varphi+a\rho^{-3/2}\cos\frac{3\varphi}{2}=f'-1. \tag{37}$$

If we find a solution for equation system (36)–(37) that corresponds to the "correct" dispersion law (35) at real $\tilde{\omega}$, this will mean that nondamping oscillations are possible in the system at these frequencies $\tilde{\omega}$. According to (35), the phase $\varphi=\pi/3$ for a real positive $\tilde{\omega}$. We then find $\rho_0=[2a/\sqrt{3}\tilde{b}]^{2/5}$ from (36) and obtain the relation

$$f'-1=\tilde{b}\frac{\rho_0}{2} \tag{38}$$

from (37) to determine the characteristic value of the alternating-field amplitude H_1^k above which magnetic-moment self-oscillations may arise. They will be damped if $\rho<\rho_0$ and grow at $\rho>\rho_0$.

The solution obtained satisfies the hypotheses made earlier:

$$kz_1\sim\left(\frac{z_1}{z_2}\right)^{1/5}\gg 1, \tag{39}$$

$$kz_2\sim\left(\frac{z_2}{z_1}\right)^{4/5}\ll 1. \tag{40}$$

The frequency of the nondamping oscillations will be

$$\tilde{\omega}\sim\frac{c^2}{3\pi^2\sigma z_1^{7/5}z_2^{3/5}}. \tag{41}$$

Since $\tilde{b}\rho_0/2\ll 1$, condition (38) is practically the same as the condition obtained earlier for instability with respect to longwave perturbations. At $f'>1$, either an aperiodic perturbation that transfers the specimen to one of the stable states or growing magnetic-moment oscillations may arise in the specimen. The question as to the existence of steady-state oscillations in the specimen must be resolved experimentally, the more

so since condition (39) cannot be satisfied in experiment.

c) Experimental observation of magnetic-moment self-oscillations

Self-oscillations have been observed on a large number of bismuth specimens,[53] most of them in the orientation $C_3 \| \mathbf{n}$, where n is the normal to the plane of the plate. The frequencies ranged from 1 to 10 kHz. The frequency range is consistent with that which might be expected on the basis of the foregoing analysis. In fact, $z_1 \sim 10^{-1}$ cm and $z_2 \sim 10^{-2}$ cm in the experiments, so that (41) gives $\tilde{\omega} \sim 10^4$ sec^{-1}.

As a rule, the oscillations were not monochromatic. A sample spectrum appears in Fig. 29. It shows that the frequencies of the oscillations increase with increasing alternating-field amplitude. This behavior was characteristic for all specimens. In some specimens, self-oscillations were observed in two H_1 ranges, and the frequency increased with rising amplitude in both of them. The frequency increase would appear to result from the increase in the field $\mathcal{H}$ and the decrease in the characteristic dimensions z_1 and z_2.

The frequency depended not only on the amplitude of the alternating field, but also on the temperature and the orientation of the specimen's crystallographic axes with respect to the high-frequency and constant fields. Special note should be taken of the dependence of the oscillation frequency on the prior history of the specimen. This implies that with all parameters held constant, the frequency depended on how the field H_0 in which the measurement was made was established. In other words, the self-oscillation frequency depended on the magnitude and direction of the specimen's intrinsic magnetic moment.

Self-oscillations can be suppressed by introducing a weak magnetic field (Fig. 30), but oscillations have been observed at high alternating-field amplitudes not only in a zero external field, but also in the range of a lateral hysteresis loop far from the coordinate origin.

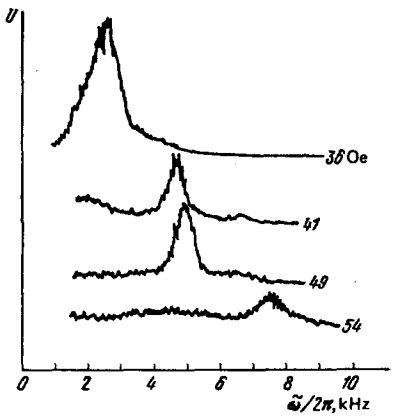

FIG. 29. Spectrum of self-oscillations in bismuth specimen. d = mm, $\mathbf{j}_1 \| C_1$, $\omega/2\pi = 1.6 \cdot 10^6$ Hz. The amplitude of the alternating field in oersteds is indicated at the end of each curve.

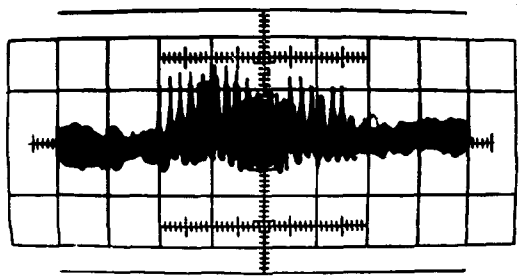

FIG. 30. Photograph from oscilloscope. Bismuth specimen, $d = 0.54$ mm, $\omega/2\pi = 2 \cdot 10^6$ Hz, $H_0 = 1.15 \sin\omega_M t$, $\omega_M/2\pi = 40$ Hz, $H_1 = 37.5$ Oe. Note the self-oscillations, which are suppressed as the magnetic field increases.

In all specimens, H_1^k exceeded the alternating-field value H_1^c at which "current" states appear. Measurements on specimens of the same quality but different thicknesses indicated that the field H_1^k increases with decreasing specimen thickness. The increase is evidently due to cutoff of the orbits dipping to large ($\sim 2r$) distances from the surface by the opposite side of the specimen. If the possibility of electron-orbit cutoff were taken into account, we should expect the appearance of self-oscillations when the alternating-field amplitude satisfies the condition $\mathcal{H}(H_1^k) \gtrsim vmc/ed$. At these amplitudes, the diameter of the electron orbit is smaller than the specimen thickness due to the magnetic field set up by the rectified current itself.

6. SURFACE IMPEDANCE AT HIGH ALTERNATING-FIELD AMPLITUDES

a) Possibility of describing nonlinear effects in metals with aid of the surface impedance

The surface impedance is an external characteristic of the medium that permits inferences as to the amplitude and phase of a reflected wave where internal microscopic processes are not of interest. If the medium is linear, the surface impedance equals the ratio of the strengths of the alternating electric and magnetic fields at the surface, $Z = E_1/H_1$; in the general case, it is a complex number. For metals $|Z| \ll 1$.

A wave reflected from a nonlinear medium is not monochromatic. In addition to the fundamental frequency, its spectrum contains multiple frequencies. Description in terms of the surface impedance is not complete in this case, but it is still frequently used.[56] Its validity requires that the amplitude of the reflected wave at the fundamental frequency be considerably higher than the amplitude of the harmonics. This is the case in metals.[57]

Let us consider the reflection of an electromagnetic wave from the surface of a metal in greater detail. At the fundamental frequency ω there is a wave incident on the surface of the metal and a reflected wave, in both of which the amplitude of electric field equals the amplitude of the magnetic field, and a wave that damps in the interior of the metal, for which the electric-field amplitude is much smaller than the amplitude of the magnetic field. To satisfy the boundary conditions, which require continuity of the tangential electric and

magnetic field components, it is necessary that the electric field in the reflected wave be in antiphase to the field of the incident wave, and that the electric components have nearly equal absolute values. (The ratio of their difference to the field of the incident wave is of the same order as the ratio of skin-layer depth to electromagnetic wavelength in a vacuum.) The magnetic components of the reflected and incident waves must be in phase.

At each of the multiple frequencies there are two waves in the metal and a reflected wave. In the latter, the amplitudes of the magnetic and electric components are equal, but inside the metal the electric field is much smaller than the magnetic field. Since the boundary condition boils down to equality of the electric and magnetic components at the surface, the surface of the metal almost coincides with the nodal surface for the magnetic field of the internal wave. Therefore the magnetic field of the waves at multiple frequencies behaves nonmonotonically within the metal. It increases as the metal is penetrated, down to the electromagnetic-field damping depth at the fundamental frequency, and only then decreases exponentially. Because the magnetic field at the multiple frequencies almost has a node on the surface of the metal, the amplitudes of the reflected waves at multiple frequencies do not exceed the electric field in the first-harmonic wave, which has entered the metal. In other words, the condition for validity of the impedance description reduces to small impedance, a requirement that is always satisfied in metals.

Even in the nonlinear case, therefore, the reflection and absorption of electromagnetic energy in metals can be characterized by a single-quantity—the surface impedance. This description is the basic approximation for the parameter $|Z| \ll 1$. The impedance is determined by the ratio of the electric and magnetic components of the electromagnetic field at the first harmonic of the frequency ω. The difference from the linear case is that the surface impedance depends on the amplitude of the wave incident on the metal. The possibility of using surface impedance does not by any means imply that the impedance change on a change in alternating-field amplitude will be small. In other words, the condition for the validity of the impedance method is not the same as the condition for validity of successive approximations. If the latter can still be used, the largest correction to the impedance arises on solution of the equations containing E_3 and H_3.

The surface impedance of a metal was studied in Refs. 4–6 as a function of the amplitude of the incident electromagnetic wave under anomalous skin-effect conditions. Thus far, there have been no theoretical studies of this subject.

b) Experimental observation of surface impedance as a function of alternating-field amplitude

Impedance has been studied as a function of alternating-field amplitude in bismuth[4] and gallium.[5,6] The experiments were designed to permit study of the frequency of an oscillator, in whose tank-circuit coil the specimen was placed, as a function of radio-frequency-field amplitude. A modulation technique was used to improve sensitivity. The frequency itself was not registered, but instead its derivative with respect to the constant magnetic field, $\partial\omega/\partial H_0 \sim \partial X/\partial H_0$, where $X = \mathrm{Im}\, Z$.

The bismuth specimens were disks, requiring measures to reduce distortion of the radio-frequency field by the specimen itself. With the object of improving the uniformity of the alternating magnetic field, the length of the induction coil was made larger than the diameter of the disk. The magnetic field H_0 was parallel to the plane of the specimen.

Figure 31 shows plots of $-\partial X/\partial H_0(H_0)$ at various alternating-field amplitudes at the surface of the bismuth. The figure shows that even at $H_1 \sim 0.2$ Oe the curves acquire a secondary maximum, which increases rapidly upon further increase of the alternating-field amplitude. The $\partial X/\partial H_0(H_0)$ relation becomes nonmonotonic at $H_1 \sim 1$ Oe. Minima appear on the curves near the point $H_0 = 0$ (Fig. 31).

In the experiments with bismuth, the frequency ω was varied from 1 to 10 MHz, but no significant influence of frequency on the shape of the curves was noted. It was determined only by the amplitude of the alternating magnetic field. Changing the quality of the surface by etching, on the other hand, resulted in a sharp change in the shape of the curves. The value of the field at which the secondary maximum appeared also depended on surface quality. When the specimen was cold-hardened, X ceased to depend on H_0 altogether. The influence of surface quality was stronger than that of the orientation of the specimen's crystallographic axes with respect to the surface.

A picture similar to those shown in Figs. 31 and 32 also persisted on polarization of $\mathbf{H}_0 \perp \mathbf{H}_1$, although the secondary peak shifted to higher fields. The nonlinear effect vanished if the constant magnetic field was oriented perpendicular to the plane of the disk. The secondary maximum depended just as strongly on temperature as in the case of the radio-frequency size-effect lines.

It might be though that the surface-impedance change observed in Ref. 4 was due to the same effects that produce the nonlinear size effect of "current" states.

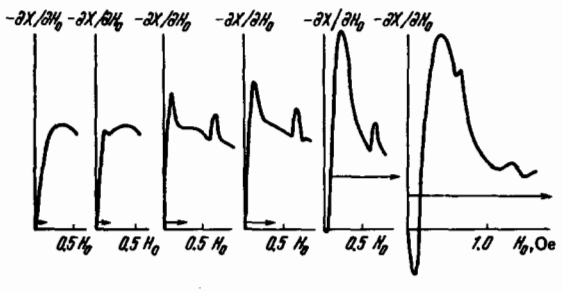

FIG. 31. Surface impedance of bismuth vs. radio-wave amplitudes. $d = 1.2$ mm, $\omega/2\pi = 4.1$ MHz, $T = 1.57$ K, $\mathbf{n} \| C_3$, $\mathbf{H}_0 \| \mathbf{H}_1 \| C_2$. The arrows indicate the amplitudes of the wave.

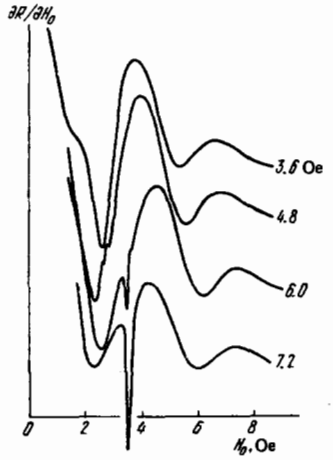

FIG. 32. Sample record of $\partial X/\partial H_0(H_0)$ curves. Bismuth specimen, $d = 0.4$ mm, $T = 1.3$ K, $\omega/2\pi = 1.27$ MHz, $\mathbf{j}_1 \| C_1$, $\mathbf{j}_1 \mathbf{H}_0 = 28°$. The amplitudes of the alternating field are indicated.

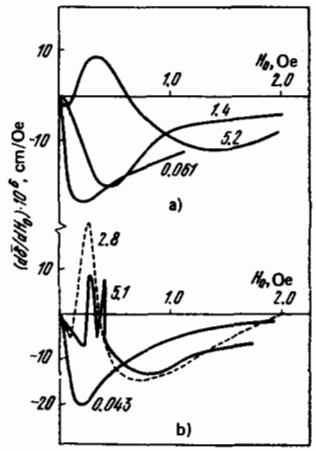

FIG. 33. Surface impedance of gallium vs. alternating-field amplitude. a) Specimen 0.394 mm thick with A axis along normal and $\mathbf{H}_0 \| C$, $T = 4.2$ K. b) Specimen with B axis along normal, $\mathbf{H}_0 \| A$, $d = 0.406$ mm, $T = 1.6$ K.

In both cases, however, the nonlinearity is highly sensitive to the orientation of the specimen's crystallographic axes and the external magnetic field, and the quality of the surface has little effect. The experimental results may be explained by the presence of surface levels[58] whose structure is realigned under the influence of the wave magnetic field. In any event, nonlinearity associated with surface levels would be highly sensitive to surface quality.

The measurements of Ref. 4 were made at comparatively low alternating-field amplitudes $H_1 < 2$ Oe. When the field amplitude is increased, it is possible to detect current states from the change in the specimen's surface impedance.[47] These measurements were made with a double T bridge that permits registration of either of the derivatives $\partial R/\partial H_0(H_0)$ or $\partial X/\partial H_0(H_0)$. The impedance jumps that correspond to the change in the specimen's magnetic moment were observed on both of these curves. Singularities of the surface-impedance derivatives appeared even before the hysteresis loops. This is seen especially clearly under conditions that give rise to a lateral hysteresis loop (Fig. 32).

In bismuth, electrons in the skin layer acquire a substantial drift velocity V_D in a comparatively weak alternating field. The order of magnitude of the current density is $j_1 = (c/4\pi\delta)H_1$. Since $j_1 \sim neV_D$, we have

$$V_D \sim \frac{cH_1}{4\pi ne}. \tag{42}$$

This quantity is comparable to the speed of sound at $n \sim 3 \cdot 10^{17}$ cm^{-3} and $\delta \sim 10^{-3}$ cm if the field amplitude $H_1 \approx 30$ Oe. We may expect the specimen's surface impedance to depend differently on the amplitude of the alternating field after the electrons reach a drift velocity equal to the speed of sound, owing to additional electron deceleration due to Cerenkov emission of phonons.[13,14,59,60] However, no breaks on the $R(H_1)$ and $X(H_1)$ curves have been observed in experiment.

The $\partial X/\partial H_0(H_0)$ relation was measured at 2 MHz and $H_1 \leq 10$ Oe in gallium.[5,6] At some H_0, the derivative $\partial X/\partial H_0(H_0)$ changed sign as H_1 increased, but narrow extremes appeared on the curves under certain conditions (Fig. 33). It is not impossible that these extremes precede the appearance of hysteresis loops associated with "current" states, in much the same way as this happens in bismuth.

Working from the fact that the impedance is influenced only by the magnetic component of the wave, Cochran and Shiffman[6] calculated $\partial X/\partial H_0(H_0)$. For this purpose, they evaluated $\bar{\delta}(H_0) = T^{-1}\int_0^T \delta(H_0 + \tilde{H}_1 \sin\omega t)dt$, where $\delta(H_0)$ is the experimental dependence obtained at small H_1 and $\tilde{H}_1$ is the effective alternating-field amplitude, $\tilde{H}_1 = kH_1$. The coefficient k was used as a fitting parameter. The $d\bar{\delta}/\delta H_0 \sim \partial\bar{X}/\partial H_0$ curves were compared with the corresponding experimental curves. It was possible to obtain qualitative agreement in this way for some curves, but even for them the calculation did not agree with experiment in details. This procedure of skin-layer-depth averaging is doubtful in itself, since δ is not an instantaneous characteristic.

7. CONCLUSION

It follows from what has been said above that nonlinearity in metals results in the appearance of various effects, even in the simplest case in which it is due exclusively to the magnetic field of the wave on the electron path. When we take this effect into account, we can understand the mechanism of alternating-current detection by metals and predict, in qualitative terms, how the magnetic moment of a metal irradiated by a radio wave will depend on the external magnetic field level. The theory enables us to describe even more subtle manifestations of nonlinearity, such as self-oscillations or the appearance of secondary lateral hysteresis loops in bismuth. All calculations were, it is true, made for a rudimentary cylindrical Fermi-surface model, and they cannot be applied directly for most metals, which have much more complex Fermi surfaces. However, the difficulties encountered in working with a real Fermi surface are technical rather than fundamental in nature.

Still, the problem of describing the nonlinear properties of metals, even under anomalous-skin-effect con-

ditions, is not completely solved. Nothing is known concerning the role of surface quality of the possible contribution of magnetic surface levels to the nonlinear effects. Nor are the causes of the nonmonotonic variation of surface impedance with increasing alternating-field amplitude understood. The situation becomes even more complicated when the frequency of the electromagnetic field is raised, since other mechanisms of nonlinearity are brought into play. Therefore the investigation of any single effect over a broad frequency range would probably make it possible to determine the frequency bands in which the various sources of nonlinearity predominate. However, measurements at higher frequencies, and microwave frequencies in particular, are thus far fragmentary.

The very important question as to the possibility of using nonlinear properties of metals for experimental or practical purposes remains open. It appears that researchers might make use of the fact that the specimen's magnetic moment and the width of the hysteresis loop in "current" states are determined by the parameters of electron groups in the immediate vicinity of isolated points on the Fermi surface.

Most of the nonlinear effects in metals are governed solely by their long carrier free paths and are general effects for any long-path plasma. As the carrier path increases, the alternating field beginning at which nonlinear effects become significant decreases, and the magnitude of the effects increases in a given field. The importance of nonlinear effects will obviously increase with frequency and with the perfection of metal crystals. There is therefore an urgent need for further study of nonlinearities, especially at higher frequencies and in extremely pure metals.

The author extends his heartfelt thanks to G. I. Babkin and V. F. Gantmakher for numerous helpful discussions and critical comments.

[1]E. S. Borovik, Dokl. Akad. Nauk SSSR **91**, 771 (1953).
[2]M. I. Kaganov, I. M. Lifshitz, and L. V. Tanatarov, Zh. Eksp. Teor. Fiz. **31**, 232 (1956) [Sov. Phys. JETP **4**, 169 (1957)].
[3]M. I. Kaganov and V. G. Peschanskiĭ, *ibid.* **33**, 1261 (1957) [6, 970 (1958)].
[4]V. F. Gantmakher, Pis'ma Zh. Eksp. Teor. Fiz. **2**, 557 (1965) [JETP Lett. **2**, 346 (1965)].
[5]J. F. Cochran and C. A. Shiffman, Bull. Am. Phys. Soc. **10**, 110 (1965).
[6]J. F. Cochran and C. A. Shiffman, Phys. Rev. Ser. A **140**, 1678 (1965).
[7]R. T. Bate and W. R. Wisseman, *ibid.* **181**, 763 (1969).
[8]W. R. Wisseman and R. T. Bate, Phys. Rev. Lett. **26**, 1492 (1968).
[9]G. I. Babkin and V. T. Dolgopolov, Zh. Eksp. Teor. Fiz. **66**, 1461 (1974) [Sov. Phys. JETP **39**, 717 (1974)].
[10]É. A. Kaner and V. G. Skobov, Usp. Fiz. Nauk **89**, 367 (1966) [Sov. Phys. Usp. **9**, 480 (1967)].
[11]G. A. Vugal'ter and V. Ya. Demikhovskiĭ, Zh. Eksp. Teor. Fiz. **70**, 1419 (1976) [Sov. Phys. JETP **43**, 739 (1976)]; Pis'ma Zh. Eksp. Teor. Fiz. **22**, 454 (1975) [JETP Lett. **22**, 219 (1975)].
[12]I. F. Voloshin, G. A. Vugal'ter, V. Ya. Demikhovskiĭ, L. M. Fisher, and V. A. Ydin, Zh. Eksp. Teor. Fiz. **73**, 1503 (1977) [Sov. Phys. JETP **46**, 790 (1977)].
[13]L. Esaki, Phys. Rev. Lett. **8**, 4 (1962).
[14]J. J. Hopfield, *ibid.*, 311.
[15]M. Ya. Azbel' and L. B. Dubovskiĭ, Pis'ma Zh. Eksp. Teor. Fiz. **5**, 414 (1967) [JETP Lett. **5**, 338 (1967)].
[16]L. B. Dubovskiĭ, Zh. Eksp. Teor. Fiz. **58**, 2110 (1970) [Sov. Phys. JETP **31**, 1138 (1970)].
[17]V. I. Bozhko and E. P. Vol'skiĭ, *ibid.* **72**, 257 (1977) [**45**, 135 (1977)].
[18]S. I. Buchsbaum and G. E. Smith, Phys. Rev. Lett. **9**, 342 (1962).
[19]M. S. Khaĭkin and A. Yu. Yakubovskiĭ, Zh. Eksp. Teor. Fiz. **60**, 2214 (1971) [Sov. Phys. JETP **33**, 1189 (1971)].
[20]M. S. Khaĭkin and S. G. Semenchinskiĭ, Pis'ma Zh. Eksp. Teor. Fiz. **15**, 81 (1972) [JETP Lett. **15**, 55 (1972)].
[21]É. G. Yashchin, Zh. Eksp. Teor. Fiz. **68**, 1127 (1975) [Sov. Phys. JETP **41**, 558 (1975)].
[22]M. I. Kaganov and V. P. Peshkov, *ibid.* **63**, 2288 (1972) [**36**, 1210 (1973)].
[23]L. É. Gurevich and O. A. Mezrik, Fiz. Tverd. Tela (Leningrad) **16**, 773 (1974) [Sov. Phys. Solid State **16**, 501 (1974)].
[24]Sh. M. Kogan, Zh. Eksp. Teor. Fiz. **64**, 1071 (1975) [Sov. Phys. JETP **37**, 544 (1973)].
[25]G. I. Leviev and É. G. Yashchin, Pis'ma Zh. Eksp. Teor. Fiz. **15**, 81 (1972) [JETP Lett. **15**, 55 (1972)].
[26]É. G. Yashchin, Fiz. Tverd. Tela (Leningrad) **19**, 1188 (1977) [Sov. Phys. Solid State **19**, 693 (1977)].
[27]L. É. Gurevich and I. V. Ioffe, Zh. Eksp. Teor. Fiz. **58**, 2047 (1970); **59**, 1409 (1970); **61**, 1133 (1971) [Sov. Phys. JETP **31**, 1102 (1970); **32**, 769 (1971); **34**, 605 (1972)].
[28]A. A. Slutskin and A. M. Kadigrobov, Pis'ma Zh. Eksp. Teor. Fiz. **28**, 219 (1978) [JETP Lett. **28**, 201 (1978)].
[29]J. M. Ziman, Principles of the Theory of Solids, Cambridge Univ. Press **278**, 1964.
[30]V. F. Gantmakher, Rept. Progr. Phys. **37**, 317 (1974).
[31]V. A. Gasparov, I. F. Voloshin, and L. M. Fisher, In: Materialy 20-go Vsesoyuznogo soveshchaniya po fizike nizkikh temperatur (Materials of the 20th All-Union Conference on Low-Temperature Physics). Part 1, Moscow, 1979, p. 5.
[32]V. L. Ginzburg and V. P. Shabanskiĭ, Dokl. Akad. Nauk SSSR **100**, 445 (1955).
[33]R. F. Greene, J. Electr. Control **3**, 387 (1957).
[34]G. I. Babkin and V. T. Dolgopolov, Fiz. Nizk. Temp. **5**, 1158 (1979) [Sov. J. Low Temp. Phys. **5**, 546 (1979)].
[35]F. G. Bass and Yu. G. Gurevich, Goryachie êlektrony i sil'nye elektromagnitnye volny v plasme poluprovodnikov i gazovogo razryada (Hot Electrons and Strong Electromagnetic Waves in the Plasma of Semiconductors and the Gas Discharge). Nauka, Moscow, 1975.
[36]É. A. Kaner and V. F. Gantmakher, Usp. Fiz. Nauk **94**, 193 (1968) [Sov. Phys. Usp. **11**, 81 (1968)].
[37]V. D. Fil', N. G. Burma and P. A. Bezuglyĭ, Pis'ma Zh. Eksp. Teor. Fiz. **23**, 428 (1976) [JETP Lett. **23**, 387 (1976)].
[38]É. N. Bogachek, A. S. Rozhavskiĭ, and R. I. Shekhter, *ibid.* 432 [391].
[39]É. N. Bogachek, A. S. Rozhavskiĭ, and R. I. Shekhter, Fiz. Nizk. Temp. **4**, 603 (1978) [Sov. J. Low Temp. Phys. **4**, 291 (1978)].
[40]É. A. Kaner, Zh. Eksp. Teor. Fiz. **44**, 1036 (1963) [Sov. Phys. JETP **17**, 700 (1963)].
[41]W. S. Boyle and G. E. Smith, Progr. Semicond. **7**, 1 (1963).
[42]L. A. Fal'kovskiĭ, Usp. Fiz. Nauk **94**, 3 (1968) [Sov. Phys. Usp. **11**, 1 (1968)].
[43]V. S. Edelman, Adv. Phys. **25**, 555 (1976).
[44]V. S. Édel'man, Usp. Fiz. Nauk **123**, 257 (1977) [Sov. Phys. Usp. **20**, 819 (1978)].
[45]V. S. Édel'man, E. P. Vol'skiĭ, and M. S. Khaĭkin, Prib. Tekh. Éksp. No. 3, 179 (1966).
[46]S. Hess, H. U. Müller, J. Schmidt, and R. Herrmann, Paper at Symposium on "Pure Substances in Science and Engineering," Dresden, 1975.
[47]V. T. Dolgopolov and L. Ya. Margolin, Pis'ma Zh. Eksp. Teor. Fiz. **17**, 233 (1973) [JETP Lett. **17**, 167 (1973)].

[48]V. T. Dolgopolov, Zh. Eksp. Teor. Fiz. **68**, 356 (1975) [Sov. Phys. JETP **41**, 173 (1975)].
[49]V. T. Dolgopolov and S. S. Murzin, Pis'ma Zh. Eksp. Teor. Fiz. **23**, 213 (1976) [JETP Lett. **23**, 190 (1976)].
[50]I. M. Lifshitz, M. Ya. Azbel' and M. I. Kaganov, Élektronnaya teoriya metallov (Electronic Theory of Metals), Nauka, Moscow, 1971.
[51]L. D. Landau and E. M. Lifshitz, Teoriya polya (Field Theory), Fizmatgiz, Moscow, 1962.
[52]L. D. Landau and E. M. Lifshitz, Mekhanika (Mechanics), Nauka, Moscow, 1965.
[53]G. I. Babkin, V. T. Dolgopolov, and P. N. Chuprov, Zh. Eksp. Teor. Fiz. **75**, 1801 (1978) [Sov. Phys. JETP **48**, 907 (1978)].
[54]V. F. Gantmacher, Progr. Low. Temp. Phys. **5**, 381 (1967).
[55]A. P. Grachnell and K. C. Wong, The Fermi-surface. Clarendon Press, Oxford, 1973.
[56]A. Blaquière, Nonlinear Systems Analysis (Academic Press, New York, 1966).
[57]L. B. Dubovskiĭ, Author's Abstract of Candidate's Dissertation. ITF Akad. Nauk SSSR, Moscow, 1971.
[58]M. S. Khaĭkin, Usp. Fiz. Nauk **96**, 409 (1968) [Sov. Phys. Usp. **11**, 785 (1969)].
[59]Yu. A. Bogod, Fiz. Nizk. Temp. **4**, 629 (1978) [Sov. J. Low Temp. Phys. **4**, 303 (1978)].
[60]Yu. A. Bogod and R. G. Valeev, *ibid.* **2**, 897 (1976) [**2**, 441 (1976)].

Translated by R. W. Bowers